Optimizing and Validating the Performance of a Low-cost Potentiostat for In-Situ Flow Battery Testing

Dharik Purohit

A Thesis in

The Department

of

Mechanical, Industrial & Aerospace Engineering (MIAE)

Presented in Partial Fulfillment of the

Requirements for the Mechanical Engineering

at Concordia University

Montreal, Quebec, Canada

March 2025

CONCORDIA UNIVERSITY SCHOOL

OF GRADUATE STUDIES

This is to certify that the thesis.

prepared by: Dharik Purohit

Entitled: Optimizing and Validating the Performance of a low-cost Potentiostat for in situ flow Battery Testing

and submitted in partial fulfillment of the requirements for the degree of

Mechanical Engineering

complies with the university's regulations and meets the accepted standards concerning originality and quality.

Signed by the final examining committee:

_____Chair

Chair's name

_____ External Examiner

Examiner's name

_____Examiner

Examiner's name

_____Thesis Supervisor

Supervisor's name

Approved by_____

Dr Sivakumar Narayanswamy, Graduate Program Director

_____2025 _____

Dr Mourad Debbabi, Dean of Faculty

Abstract

Optimizing and Validating the Performance of a Low-cost Potentiostat for In-Situ Flow Battery Testing

Dharik Purohit

This thesis relates to the design, optimization, and validation of a low-cost potentiostat tailored specifically for the requirements of flow battery testing. The primary objective is to deliver a reliable solution that maintains high-performance standards necessary for precise electrochemical measurements, achieved through simplified circuit design, affordable components, and open-source software.

The potentiostat design incorporates an expanded compliance voltage of ±2.5V, dynamic current range selection using a multiplexer, and enhanced noise filtering for accurate operation in aqueous systems and microelectrode setups. The system's functionality was further extended with the addition of features like two-way pulse testing and battery charge-discharge testing over multiple cycles. Comprehensive performance validation was conducted to ensure the potentiostat meets the requirements for electrochemical applications, with tests focused on accuracy, stability, and flexibility across a range of experimental conditions.

The **CellStat**'s design specifications were derived through simulations and theoretical calculations, including the assessment of compliance voltage, DAC/ADC resolution, and projected measurement errors. These theoretical benchmarks were validated through cyclic voltammetry experiments under varying scan rates, showcasing the potentiostat's ability to reliably measure and control redox reactions in flow batteries. The work highlights the potential for low-cost, open source potentiostats to meet the growing demand for accessible electrochemical testing tools, supporting advancements in renewable energy technologies.

Contents

Table of figures

List of tables

List of acronyms

ACV - AC Voltammetry
ADC - Analog to Digital Converter
CA - Chronoamperometry
CC - Chronocoulometric
CP - Chronopotentiometry
CV - Cyclic Voltammetry
CE - Counter Electrode
DPV - Differential Pulse Voltammetry
DAC - Digital to Analog Converter
FAM - Fast Amperometry
FCV - Fast Cyclic Voltammetry
FTIR - Fourier Transform Infrared
LSP - Linear Sweep Potentiometry
LSV - Linear Sweep Voltammetry
MA - Multistep Amperometry
MP - Multistep Potentiometry
MUX - Multiplexer Switch
MPAD - Multiple-Pulse Amperometric Detection
NPV - Normal Pulse Voltammetry
NMR - Nuclear Magnetic Resonance
OCP - Open Circuit Potentiometry
EIS/GEIS - Potentiostatic/Galvanostatic Impedance Spectroscopy
IMPE - Potential Scan
PAD - Pulsed Amperometric Detection
RE - Reference Electrode
SWV - Square Wave Voltammetry
SOC - State of Charge
SOH - State of Health
SCP or PSA - Stripping Chronopotentiometry
WE - Working Electrode
ZRA - Zero Resistance Amperometry

Chapter 1: Introduction

1.1 Context

Chemical engineering research spans many technologies, including the pursuit of more sustainable electrochemical energy storage devices [1]. Among these, research in batteries for both consumer applications and large-scale industrial applications has experienced notable growth over recent decades [2].

The primary driving force for the increased interest in large-scale batteries is the transition to sustainable energy. To prevent further global warming caused by the burning of fossil fuels, many countries around the world are prioritizing renewable energy sources such as wind and solar for new electricity-generating power plants. As fossil fuels and coal industry demand diminish and intermittent sustainable energy installations such as solar and wind grow, there is a larger need for storage solutions. This is a progressive change in the energy market that needs to be addressed [3]. While fossil fuels have the benefit of being a physical object that can be stored and become energy at any point the user demands it, excess electricity from solar and wind installations needs to be stored in batteries and discharged later. This problem becomes economically more difficult when trying to scale up to large power plants [4]. For this reason, considerable research efforts are being devoted to developing affordable ways to store renewable energy in the form of batteries.

Flow batteries are of interest as a solution to the energy storage dilemma because, unlike conventional solid batteries, they are open systems capable of accepting more energy content in the form of electrolytes. This open system architecture means that it is possible to increase their energy capacity by simply increasing their tank sizes. This scalability leads to lower overall storage system costs, particularly important for energy storage applications where cost is the key metric.

Figure 1: All iron flow battery systems made by ESS Inc.

1.2 Flow Batteries

Flow batteries utilize two different electrolytes stored in external tanks and pumped into cells with two separate electrodes where each electrolyte can be reversibly charged and discharged. In addition, each cell has a specialized membrane between the electrodes that allows ions to travel from one electrolyte to the other. The efficiency and performance of these batteries are dependent on many electrolyte properties such as the pH, viscosity, SOC(state of charge), SOH(state of health), and temperature. These properties therefore need to be monitored for battery maintenance, especially for the large-scale battery systems used for grid storage.

Large-scale flow battery systems, featuring big tanks and pumps, are expensive but worthwhile investments for grid storage if they can last at least 20 years. Operational maintenance is therefore crucial for these systems. Fortunately, flow batteries are open systems, allowing the electrolytes to be monitored and replaced to increase their longevity and ensure reliable performance. Sensors can track various parameters, such as SOC, flow rates, and temperature, which are used to optimize flow battery operation.

Many tools and techniques are available for the chemical analysis required to monitor flow battery electrolytes. Unfortunately, many of these are expensive and require too much space for lab scale research. Researchers are attempting to overcome this challenge by developing lower cost and smaller footprint techniques and equipment for electrolyte characterization.

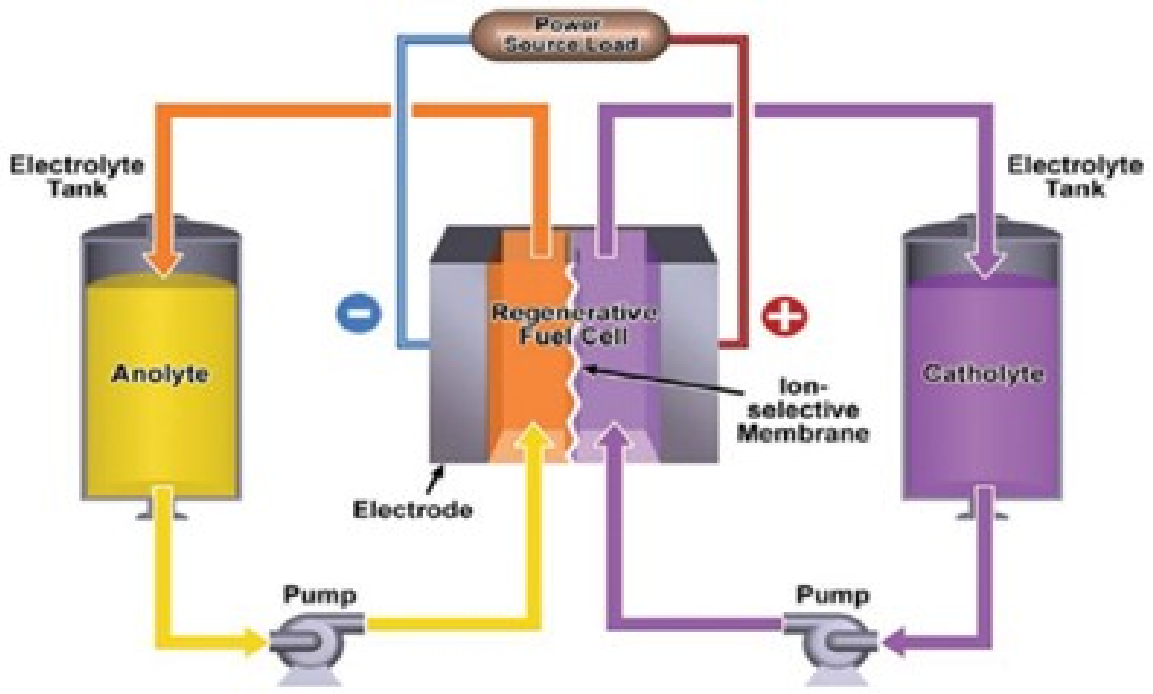

Figure 2:Operating principle of a redox flow battery [5].

1.3 Electrochemical Characterization

In contrast to conventional batteries, another advantage of flow batteries is that they allow access to the electrolyte. Not only can electrolytes be accessed for sampling and ex-situ chemical analysis, but some instrumentation can be directly installed 'inline' with the electrolyte flows, allowing for real-time monitoring of certain electrolyte properties.

Among the purely chemical analysis techniques, several of them rely on spectroscopic measurements, such as Raman spectroscopy, Nuclear magnetic resonance (NMR), UV/vis and Fourier Transform Infrared (FTIR). Raman testing is done via measurement of energy differences between scattered light and the incident beam of a laser. It is used mostly in the investigation of solid surfaces but has also been applied for finding the state of charge of a flow battery and to gain information on the molecular structure of electrolytes. Nuclear magnetic resonance (NMR) spectroscopy is a useful tool for finding the flow cell battery's chemical structures, molecular dynamics, and concentration. Its measurement principle is based on the quantization of the nuclear spin, which results in a splitting of the corresponding nuclear energy levels in an external magnetic field. UV/vis spectroscopy gives limited information compared to other techniques explained, but it is used to find the concentration of solutions this is done by viewing the range and absorption of wavelengths of the sample. The intensity can give a scale value of the concentration of charged and discharged ions in a solution [6]. FTIR spectroscopy is an analytical technique used to obtain the infrared spectrum of absorption or emission of a solvent. The technique can identify molecular bonds and structures in a sample of interest. It uses infrared radiation as the primary excitation source. The absorption over a wavelength characterizes the molecule for the user [7]. Unfortunately, all these spectroscopic techniques require dedicated equipment with costs ranging from 10,000 to 1,000,000 CAD.

As opposed to the spectroscopic techniques above, electrochemical characterization involves electrochemical reactions with the electrolyte to measure the concentrations of reactants. These are performed with the help of galvanostats, potentiostats or two-electrode electrical devices such as battery cyclers. For example, battery cyclers are typically used to charge and discharge the electrolyte, thereby changing its SOC. Cell cycling is a simple test that gives the response curve of the current over a certain voltage over time. Additionally, using the coulomb-counting method, cell capacity can be determined, and the SOH of the limiting electrolyte can be estimated.

In a galvanostat, the current is controlled while the potential is measured as it changes over time, whereas in potentiostats the voltages are controlled while the current responses are measured. Potentiostats are three-electrode systems capable of measuring the response of a working electrode (WE) versus a reference electrode (RE) and are therefore commonly used for tracking electrolyte properties with respect to that reference. One of the ways this is done is by the cyclic voltammetry (CV) technique where the potential of a working electrode is cycled linearly with time between two set values while measuring the resulting current. This potential sweep is often conducted in both the forward and reverse directions, creating a cyclic voltammogram. The resulting voltammogram provides information about the oxidation and reduction processes of the electrolyte, including the number of electrons transferred, reaction kinetics, and diffusion coefficients [7].

Unfortunately, most commercial potentiostats cost in excess of 1000$, thereby making it prohibitive for academic researchers to dedicate such equipment to monitoring a single battery electrolyte. Developing cheaper alternatives is key for reducing the barrier of entry for flow cell research and the primary goal of this thesis.

1.4 Thesis goals

This thesis aims to design, develop, and validate a low-cost potentiostat tailored for flow battery electrolyte testing, hereby named **CellStat**. The overall goal is to create an affordable, reliable, and user-friendly device that can meet the precise electrochemical measurement needs of researchers and engineers. The thesis components consist of:

- A review of potentiostats theory (Chapter 2)
- A review of current potentiostats on the market (Chapter 3)
- Prototyping and Assembly of the Potentiostat (Chapter 4)
- Calibration the Potentiostat (Chapter 5)
- Validation in a Laboratory Setting (Chapter 6)

Chapter 2: Theory

2.1 Anatomy of the flow cell batteries

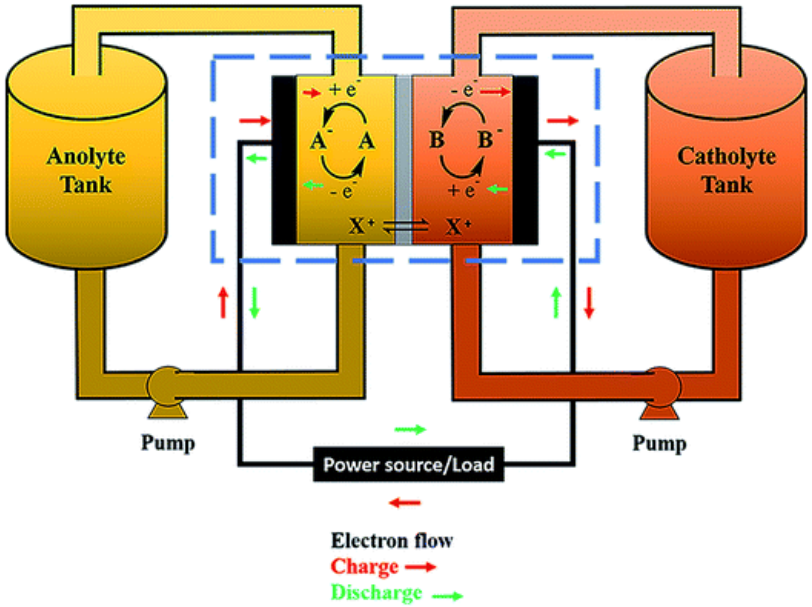

Figure 3: Simple example diagram of the flow cell battery that can charge and discharge [7].

Redox flow batteries are designed to efficiently convert electrical energy to chemical energy and store this energy in the form of two liquid electrolytes. A flow battery consists of two reservoirs that hold electrolytes in which the reactants are dissolved, and the cells where these reactants are charged and discharged. The reactants act as the electron receivers and electron donors. The electrolytes are ionic solutions permitting the reactants to be pumped through the cell. Although the electrolytes used in this work are aqueous based, non-aqueous organic solvents have also been used in flow batteries but are not ideal due to cost [8]. The cell or reactor acts as the location to charge and discharge the electrolytes by flowing them through two separate electrodes. These electrodes ideally have a high electrical conductivity and good porosity to reduce efficiency losses. Like any conventional solid-state battery, charging is done by an external power source, while reverse discharging is done by connecting the battery to a power load. A membrane is located between the two electrodes and ensures that the charge can be transferred from one electrode to the other while ensuring the two electrolytes do not contaminate each other. An ideal membrane has a high conductivity and low reactant permeability. Electrodes, electrolytes, and membranes are all critical flow battery components that are constantly under development to improve the overall performance, stability, and cost of these devices.

2.2 Battery Operation

To explain how flow batteries operate it is necessary to understand more about the underlying electrochemical phenomena that are involved. Whether it is the reaction mechanisms, the conduction of ions, or the transport of reactants to the electrode, these phenomena all result in some form of voltage loss.

All electrochemical reactions occur in pairs, where reactants at one electrode are reduced by gaining an electron while the reactants at the other electrode are oxidized by losing an electrode. These reactions occur when a voltage between the electrodes provides enough potential energy for electrons to move from one reactant and electrode to the other. The following equation gives a general example of electron transfer [7].

$$A^{(\alpha-n)+} \leftrightarrow A^{\alpha+} + ne^- \qquad E^0 = E^0_{anode}\, vs. SHE$$

$$B^{(\beta)+} + ne^- \leftrightarrow B^{(\beta-n)+} \qquad E^0 = E^0_{cathode}\, vs. SHE$$

$$A^{(\alpha-n)+} + B^{(\beta)+} \leftrightarrow A^{\alpha+} + B^{(\beta-n)+} \qquad E^0_{cell} = E^0_{cathode} - E^0_{anode}\, vs. SHE$$

The symbols in the above equation are defined as: $A^{(\alpha\text{-}n)+}$ and $A^{(\alpha)+}$ represent species A's oxidized and reduced forms. The term α represents the charge on the oxidized form of A, and n is the number of electrons transferred in the reaction.

$B^{(\beta)+}$ and $B^{(\beta\text{-}n)+}$ represent species Bs oxidized and reduced forms. The term β represents the charge on the oxidized form of B, and n is the number of electrons transferred in the reaction.

e^-: This symbolizes an electron.

E^{0_anode} and E^{0_catode}: These are the standard electrode potentials for the reactions at the anode and cathode, respectively, referenced against the Standard Hydrogen Electrode (SHE).

E^{0_cell}: This represents the standard cell potential, which is the difference between the standard cathode potential and the standard anode potential. In other words, the thermodynamic voltage of the electrochemical cell.

SHE: Standard Hydrogen Electrode, a reference point against which the standard electrode potentials are measured.

The ease with which electrochemical reactions and electron transfer occur relates to the kinetics of reactions. Many flow batteries, such as those being used in this work, involve reactants with fast kinetics that do not contribute significantly to voltage loss and will not be discussed further here.

For both oxidation and reduction reactions to occur at each electrode, the electrons must travel through the external circuit. This movement of electrons through the external circuit is represented

as a current through resistance or load, which will produce a loss in voltage, according to Ohm's Law ($\Delta V = I \cdot R$, where V is the applied voltage from potentiostat, I is the current detected by the potentiostat by CE electrode, and R is the resistance of the cell). This means that the voltage drop (or loss) in the circuit is directly proportional to the current flowing through the circuit and the resistance of the circuit.

In addition to electron flow through the external circuit, ions must also migrate within the electrolytes to conserve the total amount of charge in an electrochemical cell. For this reason, electrolytes and ion-conducting membranes are designed to have high mobility of their constituent ions. In general, the ohmic loss in power devices such as flow batteries primarily comes from the resistance within the ionomer membranes, which can impede ion movement and cause additional voltage drops.

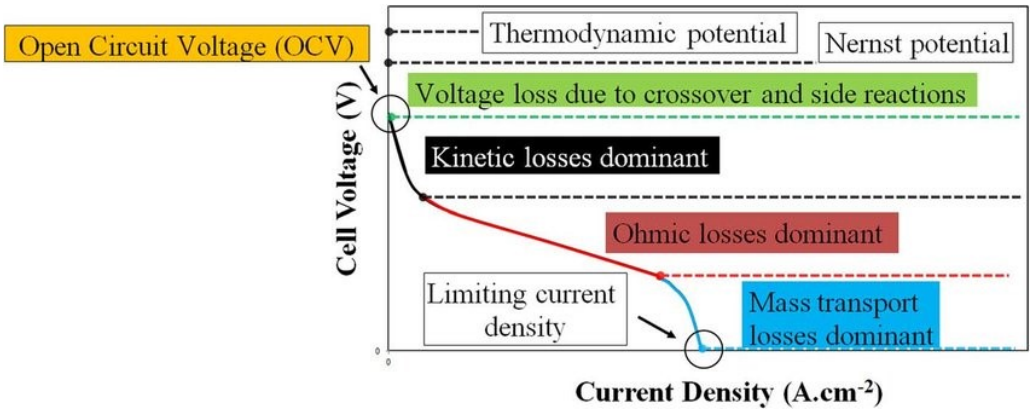

Figure 4: Example of a polarization curve for flow cell battery [7].

There are several ways energy is lost in a flow cell. Thermodynamic potential losses refer to a decrease in the equilibrium (thermodynamic) potential of a cell due to temperature changes. Voltage losses occur due to crossover of reactive species from the anode to the cathode sides through the membrane without participating in the intended electrochemical reaction. Kinetic losses are associated with the rate of the electrochemical reactions occurring at the electrode surfaces and relate to the activation energy barriers associated with the kinetic complexity of the reaction mechanism (such as how many reaction steps are involved). Mass transport losses refer to the inefficiencies in the movement of reactants and products to and from the electrode surface and are related to the diffusion, convection, and migration of these species in the electrolyte. Lastly, ohmic losses are due to both the electrical and ionic resistance of the cell components when the current is flowing.

2.3 Potentiostat testing equipment.

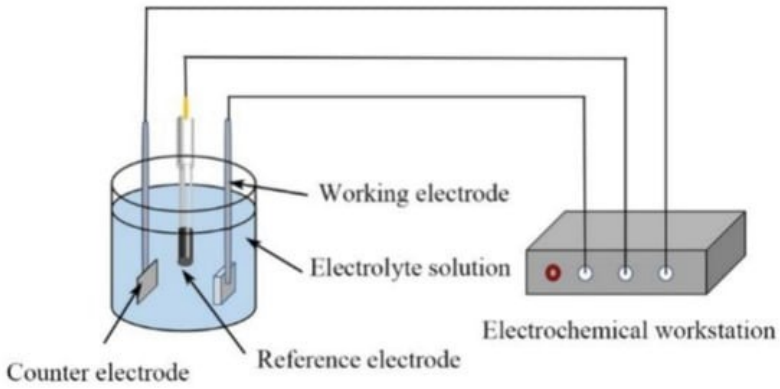

Figure 5: Potentiostat testing setup for cyclic voltammetry [9].

The potentiostat in Fig. 5 depicts the key components used in three electrode tests: the counter electrode, the working electrode, and the reference electrode. This section will review these electrodes and their function during cyclic voltammetry tests. The reason for focusing on cyclic voltammetry is that it is commonly used for finding the state of charge.

The working electrode (WE) is the electrode at which the reaction of interest is being studied. The potentiostat controls the voltage of this electrode with respect to the reference electrode and measures the current flowing through the WE. Whether it is nanoamps (nA) or milliamps (mA), the amount of current that flows through the WE are proportional to and therefore can be controlled by, the surface area of the WE. The material of the WE will depend on the electrochemical reaction being studied. If the purpose of the test is to characterize the redox electrolytes used in flow batteries, inert carbon or graphite materials are often used.

The reference electrode (RE) acts as a defined stable potential to be used as a reference point against which the potential of the WE can be set. To maintain a stable reference, the RE typically has its electrolyte solution is separated from the cell electrolyte by a porous material (e.g. glass frit) to minimize contamination of the electrolyte. To work properly, no current is allowed to flow through the RE. Some examples of commercially available electrodes are saturated calomel electrodes (SCE), standard hydrogen electrodes (SHE), and the Ag/AgCl electrode [10].

The counter electrode (CE) provides the current that passes through the WE. Typically, the CE surface area is larger than the WE so that it can operate near equilibrium and therefore avoid requiring a large overpotential.

Normally potentiostat testing is done *ex situ*, where the solutions are taken out of the flow cell reservoir and placed in a testing facility to monitor the results. However, recent studies have demonstrated *in situ* testing by in-line measurements of flowing electrolytes.

2.4 Experimental parameter measurements (diffusion, SOC, SOH, redox potential, CVs)

This section will explain how a potentiostat can be used to measure the SOC and diffusion properties of a flow battery electrolyte through cyclic voltammetry. Cyclic voltammetry is done by inputting a starting voltage, moving at a constant rate (E.g.: mV/s) to a second voltage point incrementally, and then returning to the first voltage point. The scan rate itself is an important experimental parameter that can be varied while the current response is measured.

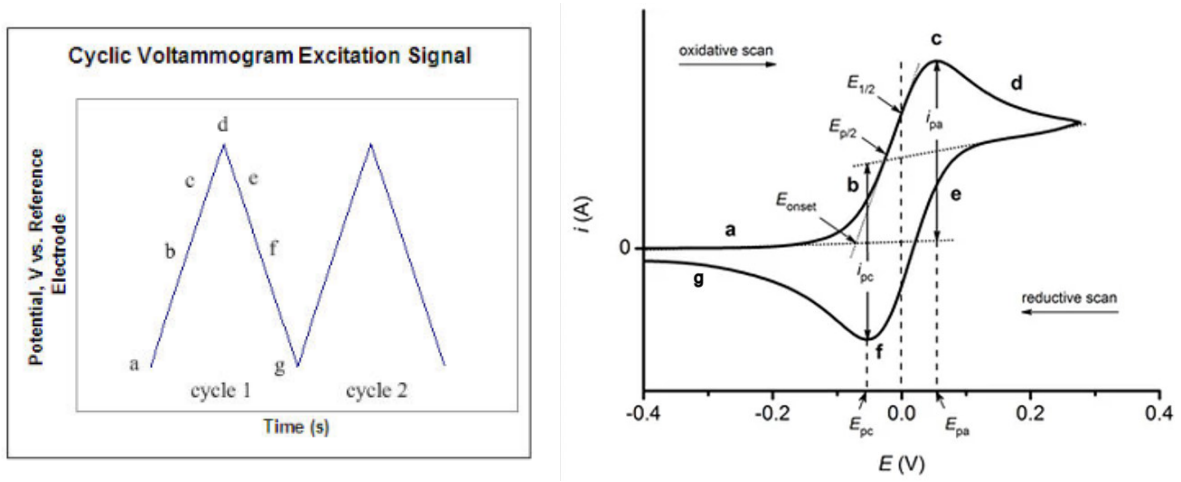

Figure 6: Cyclic voltammetry example. The Left shows the potentiostat input over time. Right shows the current responses over the voltage [11],[12].

The current response to voltage changes during an electrolyte test is recorded and typical output is shown in Fig. 6. The cyclic voltammetry (CV) plot reveals two distinct peaks. The first peak, observed from **a to d**, corresponds to the oxidation of the redox species in the electrolyte. The second peak, occurring from **d to g**, represents its reduction. The state of charge (SOC) of the electrolyte can be measured by calculating the ratio of these two current peaks, providing insight into the redox activity of the system.

2.5 Electrical Components Theory

The key functionality of a potentiostat is the ability to control the potential of the WE with respect to the RE by setting the potential difference between the WE and CE. This is achieved with the help of circuit elements such as the operation amplifier (op-amps) used in different configurations: voltage follower configuration, feedback loop configuration, and trans-impedance amplifier configuration.

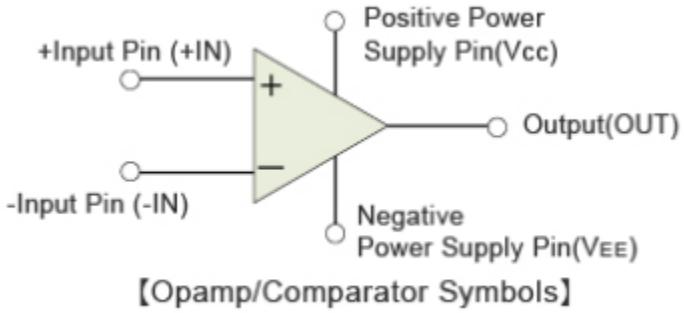

Figure 7: Operation amplifier simplified schematic [13].

An op-amp is a versatile electronic component used for signal amplification. It has two input pins, the non-inverting input (+IN) and the inverting input (-IN), as well as an output pin (OUT), a positive power supply pin (Vcc), and a negative power supply pin (VEE). The op-amp amplifies the voltage difference between the +IN and -IN pins, with the output voltage determined by the equation $OUT = A \times (V_{+IN} - V_{-IN})$, where A is the open-loop gain of the op-amp.

A key concept in the operation of op-amps is the use of feedback loops, which control the behavior of the amplifier. Negative feedback occurs when a portion of the output signal is fed back to the inverting input (-IN). This feedback tends to stabilize the output and reduce the gain to a controlled value, depending on the external components like resistors and capacitors. Negative feedback is fundamental to achieving precise and stable gain in various op-amp configurations. In the electrochemical case, the negative feedback loop ensures the voltage difference between the WE and the RE gives the desired voltage.

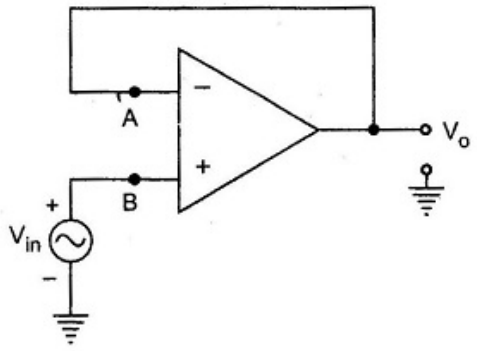

Figure 8: Voltage follower schematic [14].

In a voltage follower (or buffer) configuration, the op-amp's output is connected directly to the inverting input (-IN), and the input signal is applied to the non-inverting input (+IN). This setup results in a gain of 1, meaning the output voltage exactly follows the input voltage. The voltage follower configuration provides high input impedance and low output impedance, making it ideal for buffering signals to prevent loading effects on the preceding stage. This configuration ensures stability and isolates the input from the output load, which is important in the potentiostat as it allows for the current decoupling of the signal input and current output.

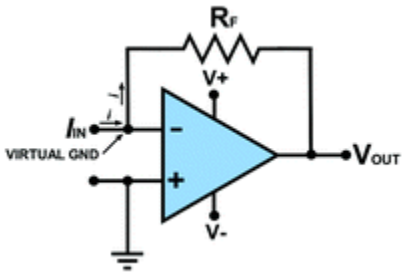

Figure 9: Trans-impedance amplifier.

Additionally, trans-impedance amplifiers (TIAs) are a specific application of op-amps used to convert a current signal into a voltage signal. This is particularly useful in photodiode applications, where the TIA converts the small current generated by the photodiode into a usable voltage. The basic TIA configuration involves connecting the photodiode to the inverting input of the op-amp, with a feedback resistor from the output to the inverting input. The non-inverting input is grounded. The output voltage is proportional to the input current, providing a sensitive and accurate conversion from current to voltage.

In summary, the voltage follower is used to decouple the current from the reference electrode, ensuring that the voltage applied remains stable without drawing current. The transimpedance amplifier converts the current output by the counter electrode into a readable voltage, reflecting the reaction rate. The differential amplifier measures the voltage difference between the reference

and working electrodes, allowing precise control of the electrochemical cell. Together, these configurations enable accurate monitoring and control of electrochemical processes.

2.5 Compliance Voltage

Compliance voltage refers to the maximum voltage that a device or system can supply or maintain across its output terminals while still functioning within specifications.

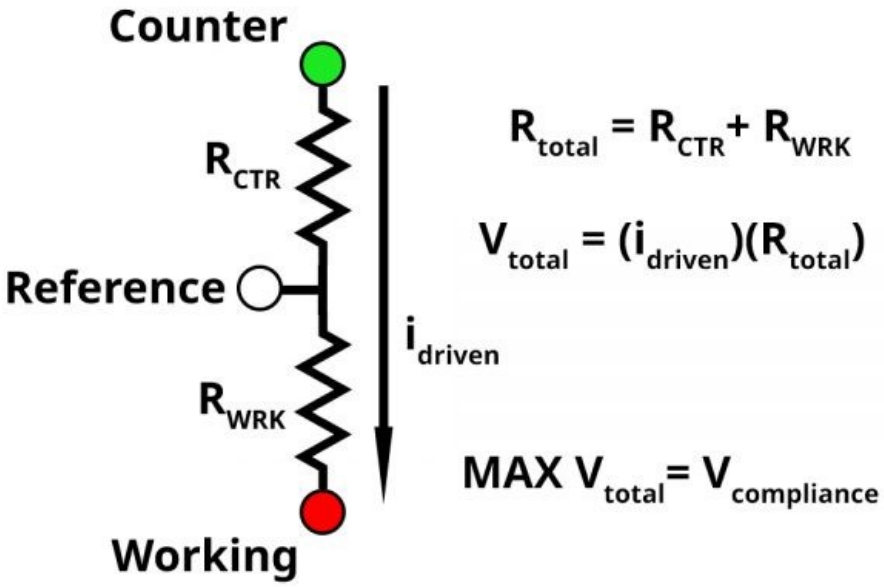

Figure 10: Cell compliance diagram [15].

To understand how a potentiostat adjusts the voltage for the reference electrode and its effective range, it is important to explain the concept of compliance voltage. Two key aspects define compliance voltage: the current flowing between the reference and working electrodes, and the potentiostats ability to maintain the desired voltage. The potentiostat ensures that the voltage difference between the reference and working electrodes matches the input voltage relative to the reference electrode. If the test cell requires an increase in current, the potentiostat adjusts by increasing the voltage, which is supplied through the counter electrode.

In the setup, the green, white, and red circles represent the counter, reference, and working electrode leads on the potentiostat, respectively. R_{CTR} represents the resistance between the counter and reference electrode, while R_{WRK} represents the resistance between the working and reference electrode [15]. For example, if R_{WRK} is 1 kΩ, applying 1 V between the working and reference electrodes results in a measured current of 1 mA, following Ohm's law. This resistance cell testing is similar to performing a bulk electrolysis experiment. If R_{CTR} is also 1 kΩ, the total resistance between the counter and working electrodes becomes 2 kΩ. To maintain a current of 1 mA, the potentiostat must apply 2 V between the counter and working electrodes—1 V more than the initial applied potential. This maximum voltage that the potentiostat can supply to maintain the desired

potential and current is known as the compliance voltage. The system works similarly to the voltage divider.

2.6 Electrochemical resistance theory

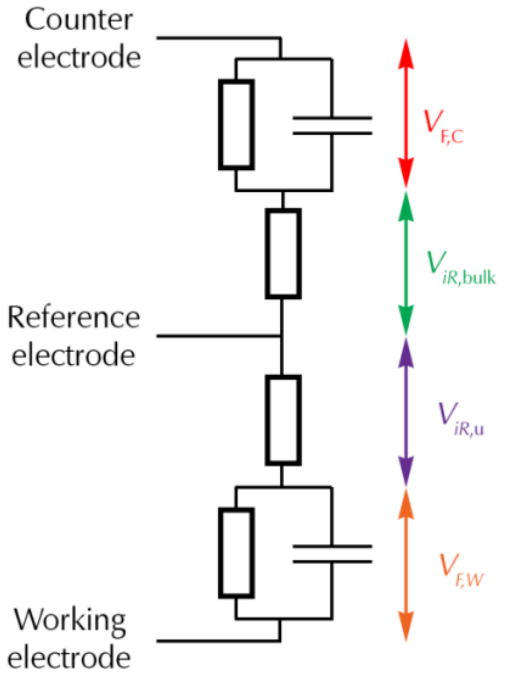

Figure 11: Distributions of voltage drops across an electrochemical cell [16].

To determine the compliance voltage needed for an electrochemical cell, four key voltage drops must be considered:

Voltage Drop at the Working Electrode ($V_{F,\,W}$): This is the voltage needed for the desired electrochemical reaction at the working electrode. In aqueous solutions, it typically ranges between -2 V to +2 V, and in non-aqueous solvents, it rarely exceeds ±3 V.

iR Drop across Uncompensated Resistance (V_{iRu}): This drop occurs between the reference and working electrode and depends on cell geometry, electrolyte conductivity, and current. It is usually around 1 V or less, but a small change in current (e.g., 10%) can alter this drop by up to 100 mV, affecting measurement accuracy.

Voltage Drop across Bulk Solution Resistance ($V_{iR,bulk}$): This relates to the resistance of the electrolyte solution itself, influenced by solution conductivity and electrode spacing.

Voltage Drop at the Counter Electrode ($V_{F,C}$): This is the voltage needed for reactions at the counter electrode, typically under 2 V. Designing a larger counter electrode relative to the working electrode minimizes overvoltage.

By estimating these components, the compliance voltage required to maintain control over the system, avoiding overloads and ensuring accurate measurements, can be calculated.

Chapter 3: Lit Review of Affordable Potentiostat Solutions in the Market

3.1 Introduction to Market Overview

There are many commercially available potentiostats on the market with a variety of specifications to suit a range of applications. However, many of these potentiostats are designed to have wider specification ranges to satisfy multiple applications and multiple markets. These wider specification windows come with increased cost, as seen in Table 1.

Table 1: Commercial bought potentiostats table [17].

Device	Data acquisition	Supported Techniques	Compliance voltage	Input Current Range	Connectivity	Price (USD)
Sensit Smart [18].	1,000 datapoints/s	LS, CV, SWV, DP, NP, CA, CC, MA, PAD, OCP, EIS	-2.0 to +2.3 V	Multiple current ranges (±100 nA up to ±3 mA)	USB-C (phone, computer)	>700
Palmsense4 [19].	150,000 datapoints/s	LS, CV, ACV, SWV, DP, NP, CA, ZRA, CC, MA, FAM, PAD, MPAD, LSP, CP, MP, OCP, SCP EIS	±10 V	Multiple current ranges (±100 pA up to ±10 mA)	Bluetooth, USB (phone, computer)	>5,000
µStat-I 400 [20].	Frequency range 1 MHz to 1 MHz	LS, CV, ACV, SWV, DP, NP, CA, ZRA, CC, MA, FAM, PAD, MPAD, LSP, CP, MP, OCP, SCP EIS	±4 V	Multiple current ranges (±1 nA up to ±10 mA)	Bluetooth, USB (computer)	>5,000
CS100E [21].	150,000 data points/s	LSV, CV, ACV, SWV, DP, NP, CA, ZRA, CC, MA, FAM, PAD, MPAD, LSP, CP, MP, OCP, EIS	±12 V	Multiple current ranges (±200 pA up to ±50 mA)	USB or Bluetooth	>2,600

To address the issue of cost, many research groups have created their own in-house customized potentiostats with limited specifications but at a fraction of the cost. Many of these designs have been published as open source[17]. The schematic shown in Fig.8 shows the common elements behind all these designs. The peripheral device, the potentiostat itself, and the testing system exist. The peripheral device is any kind of visual feed of the results. The methods of seeing and processing the results can be done here. If there are multiple potentiostats this device can communicate with each of them. The potentiostat consists of the microcontroller and the components that ensure that testing techniques are as accurate as possible. The microcontroller has its own programs to run distinct types of tests within the system and communicate with the components.

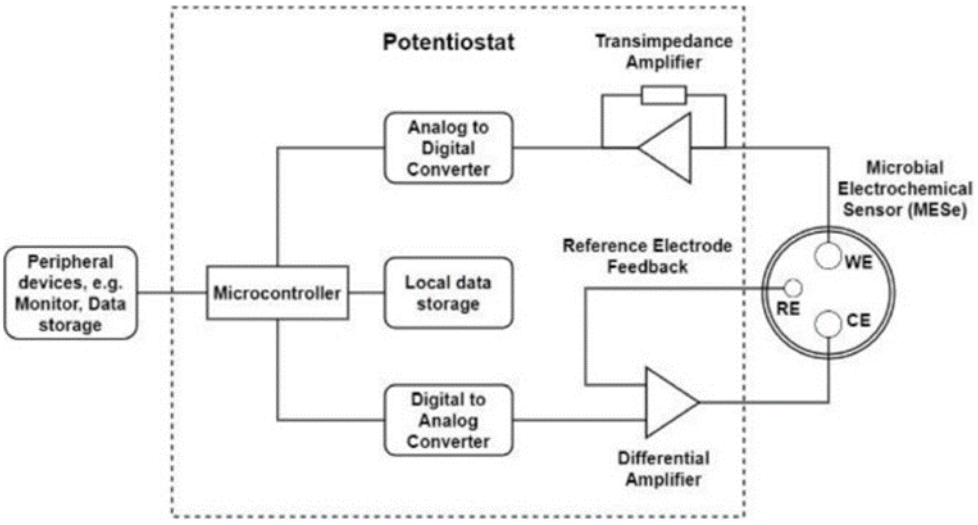

Figure 12: Diagram of a typical potentiostat system interface [22]

To simplify DIY potentiostat designs, researchers typically follow these principles: A microcontroller controls the voltage applied to the counter electrode, with the desired voltage input to an op-amp in a voltage follower configuration to ensure no current is drawn. The reference electrode is connected to another voltage follower to decouple the cell current and reference voltage. The reference voltage is fed to a differential amplifier to adjust for electrode losses. The working electrode connects to a transimpedance amplifier, converting current to voltage, which an ADC (analog to digital converter) then reads.

3.2 Review of Common Low-Cost DIY Potentiostat

Some commercial potentiostats are differentiated by the range of testing techniques they support and their high price points. The ability to perform various electrochemical tests, such as cyclic voltammetry, impedance spectroscopy, and chronoamperometry, often justifies the higher cost. When considering these devices, it is crucial to assess the key features and performance factors that make commercial potentiostats superior, such as precision, stability, and versatility in handling different applications. Understanding these factors can guide the selection of the most suitable potentiostat for specific needs.

Understanding potential capabilities can be done by first reviewing the data of already made low-cost potentiostat. Table 2 explains the common parameters and the differences in the low-cost DIY potentiostat market. Most of the testing techniques are not necessary for the current design but are still implemented in other research fields. This is important to see what technique can be stripped to reduce cost during the design phase. The Cellstat will be primarily used for monitoring flow battery electrolytes via cyclic voltammetry and hence CV is the most important functionality for the device.

Table 2: Review of open-source potentiostats developed by academic research groups [17]

Device	Data acquisition	Supported Techniques	Compliance voltage	Input Current Range	Connectivity	Price (USD)
UWED [23].	20 samples/s	LS, CV, SWV, DP, CA, CP	±1.5 V	±180µA	Bluetooth (phone)	60
Dstat [24].	30,000 samples/s	LS, CV, SWV, DP, CA, CP	±1.5 V	Multiple current ranges (±1 µA up to ±100 µA)	USB (computer)	100
Cheapstat [25].	Frequency Range:1–1000 Hz	LS, CV, SWV	±990 mV	Multiple current ranges (±100 nA up to ±10 µA)	USB (computer)	80
Enactsense [26].	2,000 samples/s	LS, CV, SWV, DP, NP, CA	±1.5 V	±10 µA	Bluetooth (phone)	100
SweepStat [27].	n.d.	CV, LS, CA, CC	±1.5 V	Multiple current ranges ±10 pA up to ±1.5 µA	USB	55
KickStat [28].	230 samples/s	CV, CA, NPV, SWV	±0.792 V	Multiple current ranges ±1.5 nA up to ±10 mA	USB	11
MYStat [29].	11 samples/s	CV, CA, SWV, OCP,	±12 V	Multiple current ranges ±2 µA up to ±200 mA	USB	226
dobbelaere et al [30].	11 samples/s	CV, CA, SWV, OCP,	±8 V	Multiple current ranges ±10 nA up to ±25 mA	USB	100
ABE-stat [31].	2,000 samples/s	CV, DPV, EIS	±1.5 V	Multiple current ranges ±0.1 nA up to ±10 mA	BLE, Wi-Fi	114
PSoC-Stat [32].	50,000 samples/s	CV, SWV, DPV	±2 V	Multiple current ranges ±2.5 nA up to ±10 mA	USB	10
SStat [33].	n.d.	CV, LS, CA, SV	±1.5 V	Multiple current ranges (±10 nA up to ±0.15 mA)	BLE	50
Rodeostat [34].	n.d.	CV, LS, SV, CVV, CA, MSV	±10 V	Multiple current ranges (±10 nA up to ±1 mA)	USB	200
PassStat [35].	82 samples/s	CV, SWV	±2.4 V	Multiple current ranges (±20 pA up to ±2 mA)	USB	140
melon et al [36].	50 samples/s	CV	±1 V	±200 µA	USB	30
JUAMI [37].	50 samples/s	CV,	±2.5 V	±20 mA	USB	40

Chapter 4: Design of the Potentiostat

4.1 Typical Potentiostat Characteristics

Some of the limitations of a low-cost potentiostat that differ from a commercially available off-the-shelf potentiostat should be noted when designing a DIY version. Table 3 compares some of the differences between commercial and DIY potentiostats.

Table 3: Comparison of commercial vs. DIY potentiostats

Features	Commercially available potentiostats	DIY potentiostats
Cost	700-5 000 CAN	10 - 226 CAN
Performance	High precision, stability, and reliability. Low-noise electronics, filters, high current, and voltage ranges.	Performance can vary on how the system is made and the quality of parts. They offer basic functions for simple experiments but may lack precision.
Features and Capabilities	Equipped with a wide range of features including EIS, differential pulse voltammetry, square wave voltammetry, and more. They also often come with software for data analysis and experiment control.	Often limited to basic features like cyclic voltammetry and chronoamperometry.
Ease of Use	Designed for ease of use with user-friendly interfaces, detailed manuals, and customer support.	Requires a good understanding of electronics and programming to build and operate. Users might need to troubleshoot and customize the software and hardware.
Documentation	Comprehensive support including customer service, technical support, training, and detailed documentation.	Limited support, primarily relying on online resources, and the user's troubleshooting abilities. Documentation might be sparse or highly technical.
Customization	Less customizable due to proprietary designs	highly customizable, allowing users to modify hardware and software to suit specific experimental needs.
Calibration	Typically comes pre-calibrated from the factory with high precision and includes automated calibration routines. They also provide certificates of	Calibration might be manual and less precise. Users need to ensure the device is properly calibrated, which can be challenging without the right tools and expertise.

	calibration ensuring accuracy and compliance with standards.	
Safety Features	Equipped with built-in safety features such as overload protection, short-circuit protection, and emergency shutoff. These features are crucial for preventing damage to the equipment and ensuring user safety.	May lack advanced safety features, relying on the user to implement necessary precautions. This can be risky, especially for high-voltage or high-current applications.

In conclusion, DIY potentiostats can give affordable and customizable options. They do lack in terms of precision and functionality. Adding new functions and components will take time to debug. While commercial potentiostat can be reliable and have professional support. The choice of using a DIY potentiostat depends on the needs, resources, and technical capability of the user.

4.2 Design Requirements

The choice of potentiostat design depends on the requirements of the users and the target application. The primary purpose of the potentiostat designed for this project is to perform voltage scans at a variety of rates and at different current ranges. More specifically, the requirements were indicated as the following:

- Voltage range: -2.5 to 2.5 V of compliance voltage.
- Current ranges: Adjustable, from ±1 nA to ±1 mA.
- Cost: less than 300 CAN

In addition to the above specifications, the following design factors were also of importance:

- Scalability
    - The use of affordable and readily available components was prioritized to ensure that the unit could be duplicated easily in the future.
- Ease of Use
    - The potentiostat should be designed for non-technical users with a self-explanatory user interface.
- Open-source system
    - open-source designs ensure that the potentiostat can be easily modified and improved later in its life cycle. Using a software code base that is widespread use in laboratories such are Arduino and Python.
- Using for microelectrodes
    - The potentiostat must be capable of accurately measuring and controlling electrochemical reactions involving microelectrodes, which are often used in detailed battery studies. Microelectrode entails that the current responses of the system can go as low as 1 nA.
- Connectivity
    - The potentiostat should be permanently connected to a computer for real-time data acquisition.

- Environment
    - The potentiostat case must be robust enough to operate in various laboratory environments, which may include humidity and potential exposure to chemical vapors.
- Durability
    - The design should focus on creating a durable device that can withstand regular use in rigorous research settings without frequent need for repairs or recalibration.

4.3 Design Selection and Integration

Based on the required specifications and design factors listed above, the list of DIY potentiostats in Table 2 was narrowed down to two choices: the Dstat potentiostat, created by the University of Illinois at Chicago, and the PassStat, created by Sorbonne Université, Paris.

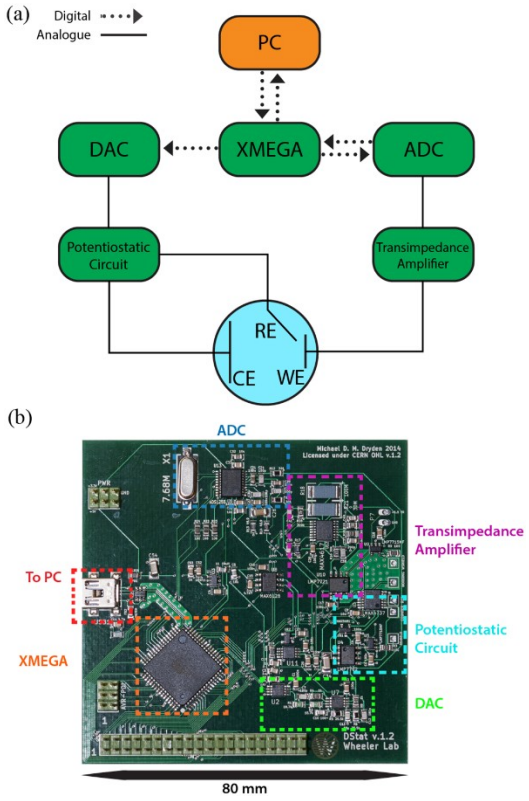

Figure 13: Dstat PCB schematics [24].

The Dstat is an open source potentiostat that is intended for general lab use and runs on the ATXMEGA microcontroller [24]. Its USB power is ideal since it means we do not need an external power supply. A few things noted for this design are the MUX used to control the current range and filter range. Multiple currents and filters can be changed via the microcontroller compared to manual use. High-end voltage dividers are used to get exactly accurate results up to 0.1 percent. The disadvantage of the Dstat is that the software and design require an intermediate level of knowledge of electrical systems and microcontroller programming which would be problematic for an academic lab with a high turnover of graduate students and projects which may require

customization. The voltage range is also only 1.65V to -1.65V, which is lower than what was needed for the electrochemical testing in this project.

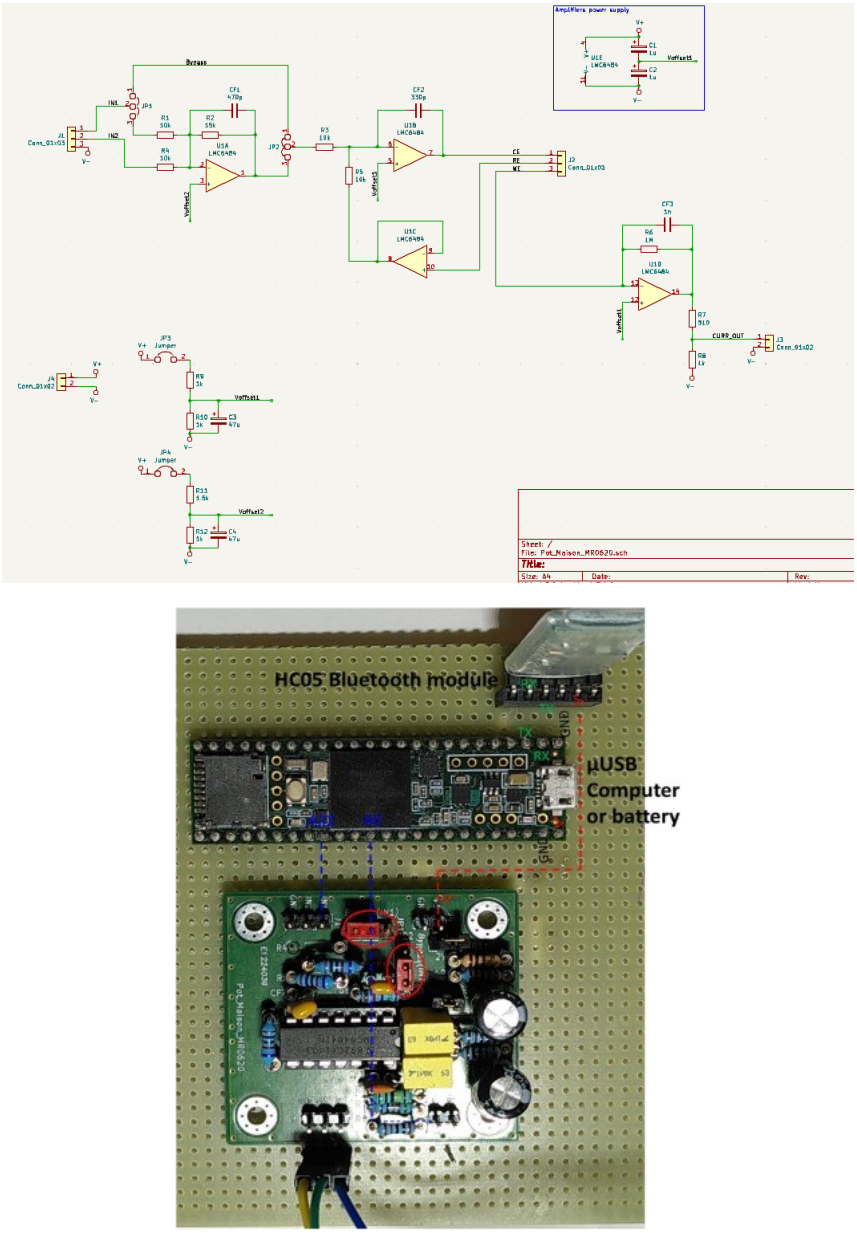

Figure 14: a) Schematic of PassStat b) PCB of PassStat [35].

The PassStat potentiostat is another open-source design, valued for its simplicity and cost-efficiency. It is particularly popular in resource-limited settings where budget constraints are a significant factor. The microcontroller is a stand stand-alone off-the-shelf product called the Teensy 3.6. which acts similarly to the Arduino and even uses the same codebase, making the code quite easy to work with. The main difference between a Teensy and Arduino is that the Teensy contains a DAC, thereby making voltage control quite simple and having a high clock speeds of 600MHz compared to 32 MHz[35] increasing scan rate times. The primary disadvantage of the PassStat design is that it requires current ranges to be changed manually via editing the PCB.

According to the design factors, the ideal potentiostat would be a combination of these two potentiostats. The hybrid **CellStat** design being developed here integrates the precise measurement capabilities of the Dstat with the cost-effective, simple circuitry of the PassStat. This approach leverages the strengths of both models to create an affordable and reliable device. Incorporating the Dstat's microcontroller-based automated control for current and filter settings enhances functionality. Using the Teensy 3.6's DAC voltage control, the hybrid model can achieve precise and automated voltage adjustments, improving overall performance and usability.

By combining the high-accuracy, automated control of the Dstat with the cost-effective, user-friendly design of the PassStat, the hybrid potentiostat is optimized for flow battery testing. The integration strategy addresses technical challenges, ensures affordability, and facilitates ease of integration with other laboratory systems for enhanced experimental efficiency and comprehensive analysis.

Building on the foundational elements of the base design, the following sections focus on the complete design and implementation of the **CellStat** potentiostat. These include the derivation of specifications, selection of components, and integration of key features to address the identified limitations. Enhancements such as the expanded voltage range, dynamic range selection via multiplexer (MUX) integration, and improved noise filtering were implemented to meet the system's performance requirements. By bridging theoretical improvements with practical design considerations, the potentiostat is optimized for precise and reliable electrochemical measurements, which will be experimentally validated later.

4.4 Base design

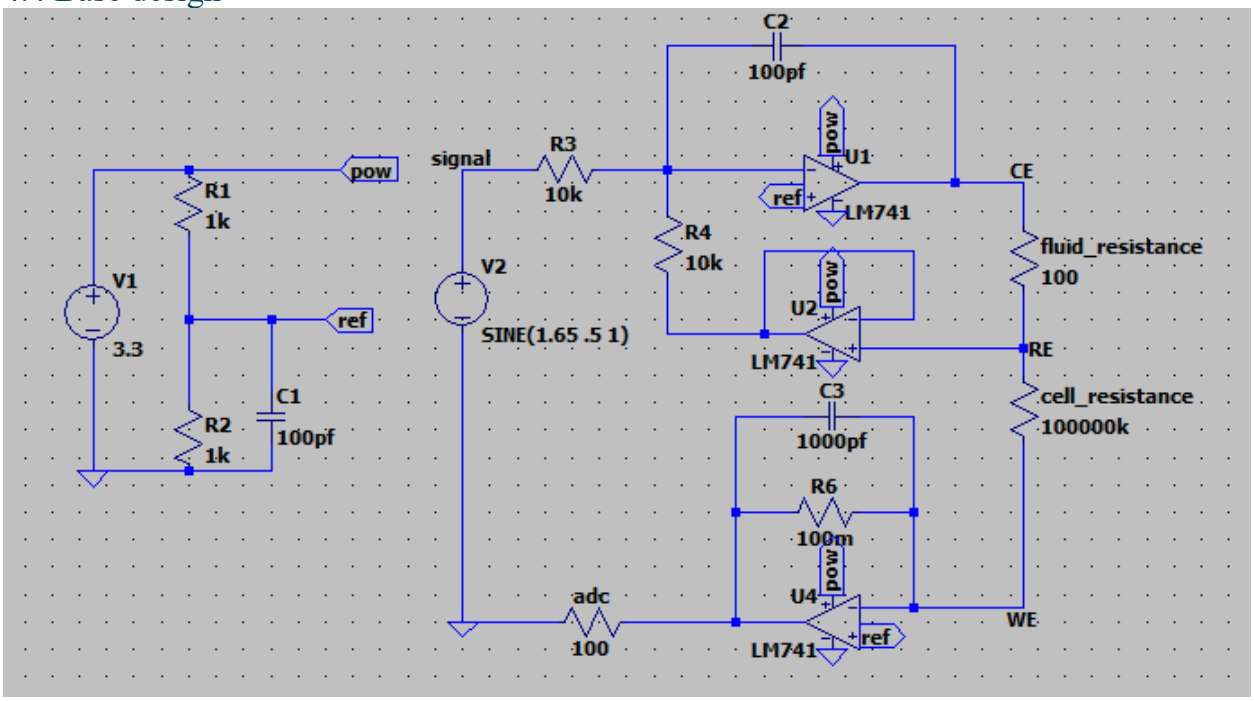

Figure 15: A simplified diagram of potentiostat schematics is in LTspice.

The circuit diagram in Fig. 15 shows the analog section of a potentiostat based on the PassStat design and serves as the baseline for the new potentiostat being developed, referred to as **CellStat**. Fig.15 illustrates the key components used for controlling the potential and measuring the current between electrodes in an electrochemical cell. This baseline circuit is crucial as it allows for initial testing, analysis, and modifications to improve performance.

The circuit consists of several key sections:

1. Reference Voltage Generation:
   The reference voltage is generated by V1 (3.3V source) and divided by resistors R1 (1kΩ) and R2 (1kΩ), providing a stable midpoint reference voltage. C1 (100pF) acts as a decoupling capacitor to stabilize the reference voltage and reduce noise.

2. Signal Input and Control:
   The input voltage, V2, generates a sinusoidal signal (1.65V offset, 0.5V amplitude, 1Hz frequency) that is applied to the system. R3 (10kΩ) limits the current entering the first operational amplifier, U1, which is configured as a buffer to maintain the input signal while isolating it from loading effects. C2 (100pF) stabilizes the feedback loop, reducing high-frequency noise and improving response time.

3. Control of Counter Electrode (CE) and Reference Electrode (RE):
   Operational amplifier U2 maintains the desired potential difference between the reference electrode (RE) and the counter electrode (CE) based on the input signal. The feedback is

stabilized using R4 (10kΩ). The fluid resistance (100Ω) represents the resistance of the electrolyte between CE and RE.

4. Control of Working Electrode (WE) and Reference Electrode (RE):
   U4 acts as a transimpedance amplifier, measuring the current flowing between the working electrode (WE) and RE by maintaining a constant potential at the WE. The current is converted into a readable voltage through R6 (100mΩ), while C3 (1000pF) filters high-frequency noise for accurate current measurement. The cell resistance (1MΩ) simulates the resistance between the RE and WE.

Figure 16 shows the results of an LTSpice simulation performed on the circuit in Fig. 15. The purpose of the simulation is to validate the baseline potentiostat design and analyze its performance under sinusoidal input conditions similar to a CV. As shown in the simulation results, the input voltage (V[signal]) and the output voltage at the working electrode (V[re]) exhibit sinusoidal behavior. However, the output signal at V[re] shows a phase inversion compared to V[signal]. This phase inversion is a characteristic of the operational amplifier configuration and highlights how the gain affects the output.

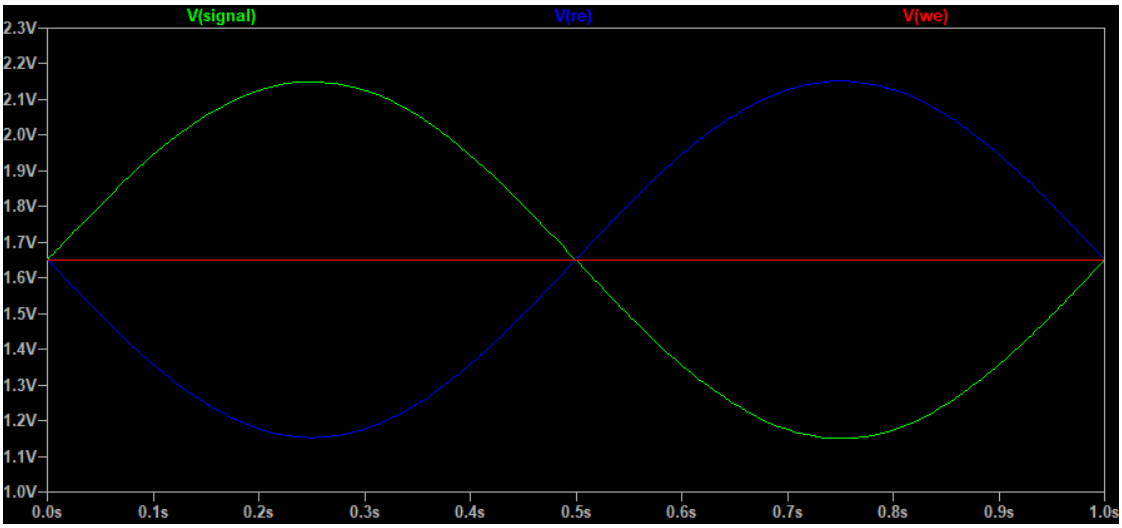

Figure 16: LTspice simulation for the potentiostat design,

4.5 Design Improvements

The current **CellStat** potentiostat developed for this thesis builds upon the PassStat base design described earlier with upgraded components and additional subsystems to meet the system requirements. Specifically, the design shown in the circuit in Fig. 17, addresses the following constraints:

1. Voltage Range and Stability: The base design had a voltage range of ±1.65 V, which proved insufficient for the electrochemical setup used in this project.
2. Range Selection: The potentiostat's flexibility across different current measurements was limited by the lack of dynamic range selection.
3. Noise Management: High sensitivity, especially for picoamp-level measurements, required a more robust noise filtering approach.

These improvements are discussed in more detail from the foundation for the prototype discussed in Section 4.3. Refer to Appendix A for the PCB diagram

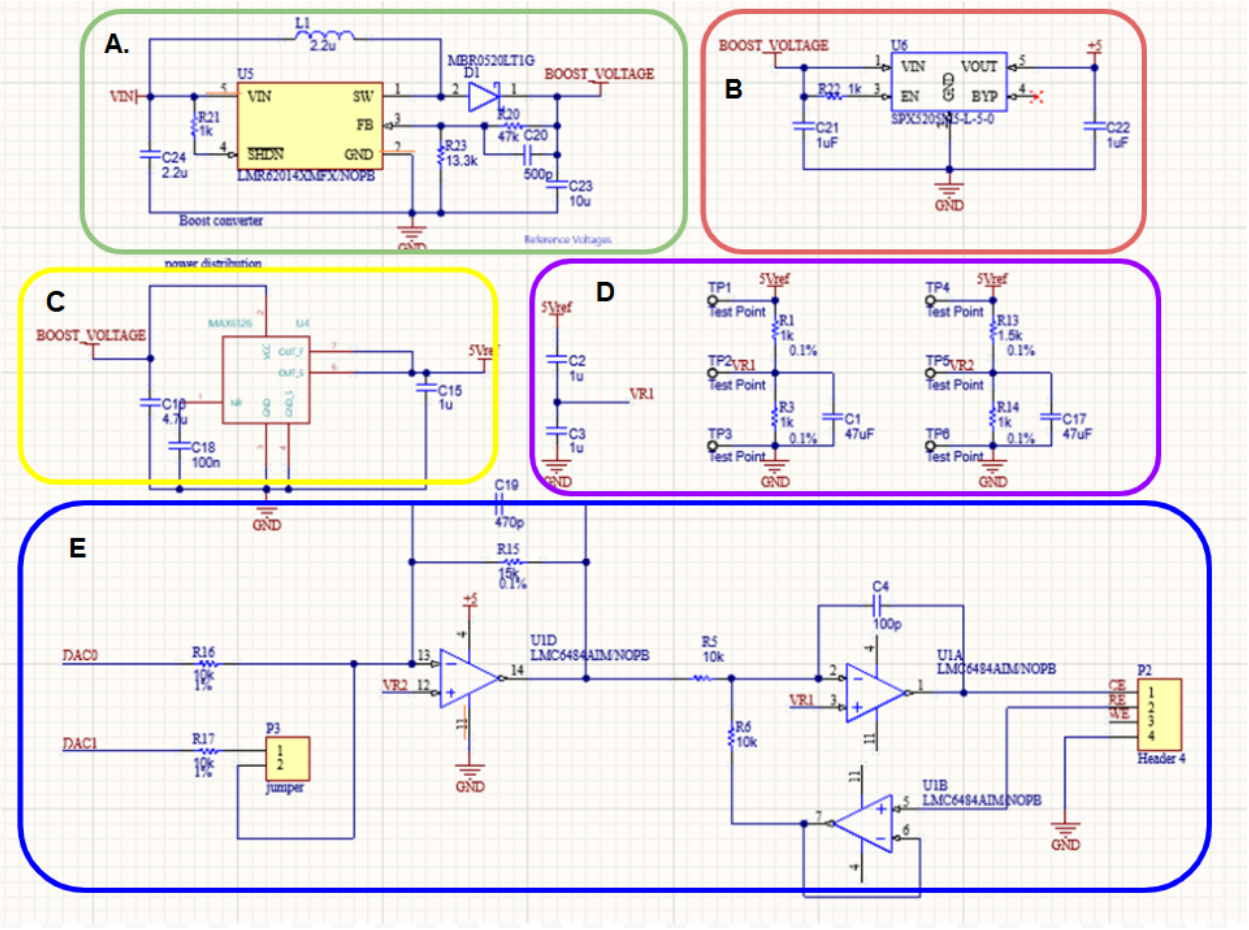

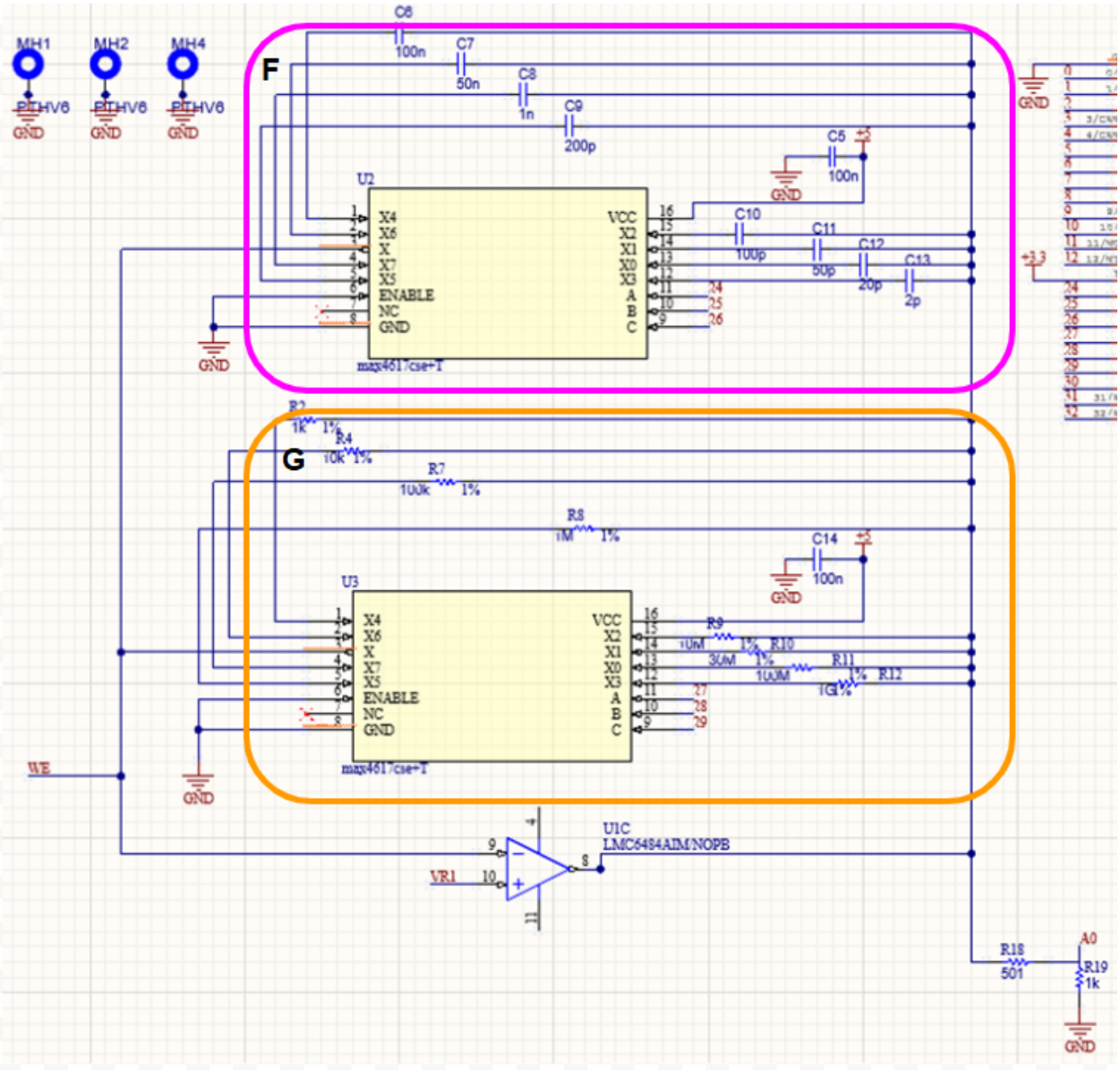

Figure 17: Hardware schematic, created in Altium Designer, detailing the practical layout for building the circuit on a printed circuit board (PCB).Subsystems are displayed in circled sections as follows: A) boost converter, B) Voltage regulators, C) 5V voltage references, D) 2.5V and 3.3V voltage references, E) operational amplifiers used for the RE and WE, F) MUX for filtering selection, G) MUX for current range selection(orange).

4.5.1 Voltage Range and Stability

To save cost and space, the **CellStat** was designed to be powered by USB. However, it was

necessary to expand the operating voltage range beyond the ±1.65V of the PassStat to meet system requirements. While the PassStat has a version capable of operating at ±2.5V, the primary limitation in its earlier design was inconsistent voltage due to regulator losses, which impacted reliable operation.

To address this, an operational amplifier (op-amp) was used in the **CellStat** to scale the voltage to ±2.5V. Although the USB input voltage typically ranges from 4.6V to 5.2V, this variability can lead to regulator losses. To ensure the output is consistently close to ±2.5V, additional regulation and stabilization were implemented. These adjustments ensure the potentiostat maintains the required headroom for stability and precision while minimizing errors caused by input voltage fluctuations.

One issue with the base design is the voltage inconsistencies caused by variations in the USB input voltage, which can range from 4.6 V to 5.2 V. To address this, boosters are added to increase the voltage to 5.3 V, as shown in Fig. 17. A voltage regulator, shown in Fig.17.C, is then used to stabilize the input voltage at 5 V. The stabilized voltage ensures consistent operation of the DACs and op-amps, improving measurement accuracy.

The regulated voltage output can be expressed as:

$$V_{out} = V_{USB} \cdot \eta_{regulator}$$

Where:

- V_{USB} is the USB input voltage
- $\eta_{regulator}$ is the regulator's efficiency which is 90 percent[38]

By maintaining V_{out}= 5 V the system eliminates voltage variations, ensuring reliable and repeatable experimental conditions.

4.5.2 Dynamic Range Selection

The addition of a multiplexer (MUX) shown in Fig.17.e allows for dynamic range selection, addressing the limitations of the base design. The MUX switches between different gain configurations, enabling the potentiostat to measure a wider range of currents. The following current ranges were implemented:

$$I_{range} = \frac{V_{range}}{R_{feedback}}$$

Where:

- V_{range} is ±2.5 V
- $R_{feedback}$ represents the feedback resistor for each range.

Table 4: Feedback resistance used for **CellStat**

Feedback Resistance	Current Range ±
1 kΩ	2.5 mA
10 kΩ	250 µA
100 kΩ	25 µA
1 MΩ	2.5 µA
10 MΩ	250 nA
30 MΩ	72 nA
100 MΩ	25 n A
1 GΩ	2.5 nA

The inclusion of these selectable ranges ensures that the potentiostat can maintain high precision when measuring currents as low as picoamps, particularly in microelectrode experiments.

4.5.3 Noise Management and Filtering

At lower current ranges, the signal becomes more susceptible to external noise. To mitigate this, a low-pass filter was implemented at the transimpedance amplifier output. A capacitor is placed in parallel with the feedback resistor, creating an RC filter:

$$f_c = \frac{1}{2\pi R_{feedback} C}$$

Where:

- f_c is the cutoff frequency
- $R_{feedback}$ is the selected feedback resistor
- C is the filter capacitor

For example, with $R_{feedback}$=10 kΩ and C=1 nF, the cutoff frequency is:

$$f_c = \frac{1}{2\pi(10 \times 10^3)(1 \times 10^{-9})} \approx 16\ kHz$$

This ensures that high-frequency noise is attenuated while maintaining signal integrity in the operating range. For picoamp measurements, the potentiostat can be placed in a Faraday cage to further eliminate external electromagnetic noise. Refer to Appendix B for a method to find the ideal capacitor.

4.6 Prototyping and Initial Testing

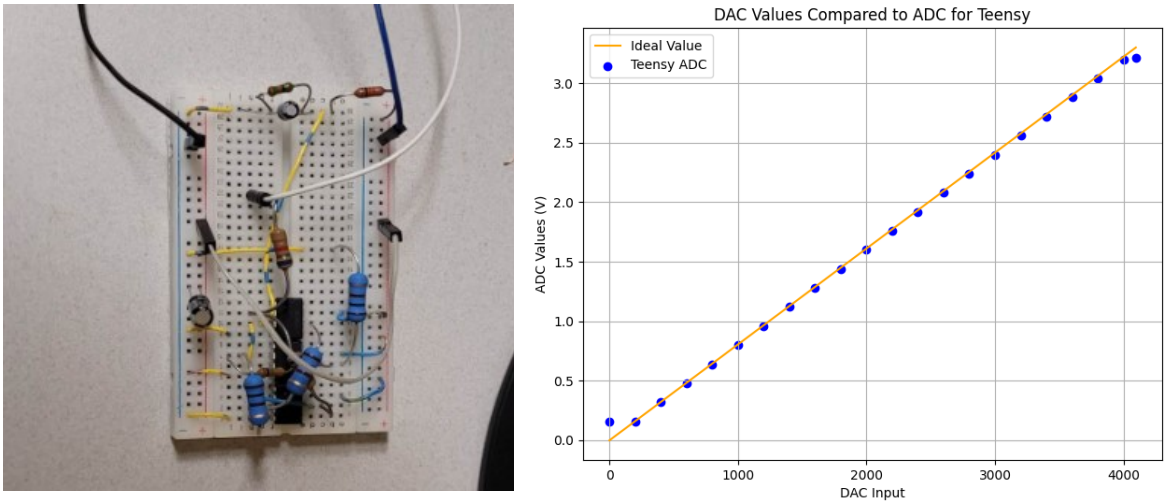

Figure 18: A) Prototype boards B) linear voltage scan result of a prototype using a 100 kΩ resistor.

The graph in Fig. 18 compares the DAC input values to the ADC output values for a Teensy microcontroller. The blue line represents the actual ADC values measured, while the orange line represents the ideal ADC values. Both the actual ADC values and the ideal values exhibit a linear relationship with the DAC input, indicating accurate tracking of the DAC input over the range tested. The actual ADC values closely follow the ideal values, demonstrating good accuracy and minimal error in Teensy's ADC measurements. The DAC input values range from 0 to approximately 4096, corresponding to ADC values from 0 to 3.3V. However, there are certain points where the actual ADC values taper off from the ideal values, particularly at lower DAC input values and at higher DAC input values, around 3500 to 4000. These minor discrepancies are likely due to voltage drops from the components on the prototype board. Despite these minor issues, the graph effectively demonstrates Teensy's ability to convert digital input to analog output and back to digital, maintaining reliable measurements across the tested range.

4.7 CellStat Specifications

Table 5 provides the final design specifications expected for the **Cellstat**, including a compliance voltage of ±2.5V and a current range from mA to nA, demonstrating adaptability to different measurement needs. **Cellstat** features a 12-bit DAC/ADC resolution (4096 steps), ensuring fine voltage control with a DAC resolution of 1.22 mV and a DAC error of ±8 bits (0.195%). The ADC range varies from 2.5 mA to 2.5 nA, with corresponding resolutions from 1.22 µA to 1.22 pA, reflecting the potentiostats wide measurement capabilities. For the cutoff frequencies for different capacitors and resistors referred to Appendix C.

The Least Significant Bit (LSB) refers to the smallest change in the analog output that can be represented by a one-bit change in the digital input. In a 12-bit DAC with a 5V full-scale range, the LSB represents an error of 8 bits. The LSB defines the accuracy of the DAC, as it indicates the smallest change in the output voltage. Ensuring fine resolution that the potentiostat can accurately measure and control minimal voltage changes. Operators can choose the resistor and capacitor values in the controller software to tailor the potentiostat for specific experimental needs, ensuring precise data by controlling the cutoff frequency of the potentiostat. For example, the cutoff frequency for a 2pF capacitor and a one kΩ resistor is 80,00 kHz. This flexibility in adjusting components is essential for achieving optimal performance in various electrochemical applications. Understanding and optimizing these specifications, including the significance of the LSB, allows for more accurate and reliable electrochemical measurements, enhancing the potentiostats overall functionality and precision.

Understanding and optimizing these specifications, including the significance of the LSB and cutoff frequency, enhances the potentiostats overall functionality and precision. These theoretical specifications, derived from simulations and calculations, will be validated experimentally in Chapter 6 to ensure their reliability and performance in real-world scenarios.

Table 5: **CellStat** Design Specifications

Compliance Voltage ±V	2.5							
Resistor Values in kΩ	1	10	100	1000	$1x10^4$	$3x10^4$	$10x10^5$	$1x10^6$
DAC/ADC Resolution	4096							
DAC Resolution mV	1.22							
DAC Bit Error (lSB) ±	8							
DAC Percent Error	0.40%							
Projected error due to DAC ±	9.76 µA	0.96 8µA	97.6 nA	9.76 nA	0.976nA	325.5 pA	97.6 pA	9.76 pA
ADC Range per Resistor ±	2.5 mA	0.25 mA	25 µA	2.5 µA	0.25 µA	83.3 nA	25 nA	2.5 nA
ADC Resolution	1.22 µA	0.12 µA	12.2 nA	1.22 nA	0.122 nA	40.6 pA	12.2 pA	1.22 pA
ADC Bit Error (LSB) ±	4							
ADC Percent Error	0.20%							
Projected error due to ADC±	4.88 µA	0.488 µA	48.84 nA	4.884 nA	0.488 nA	162.76 pA	48.84 pA	4.88 pA
total projected error ±	14.64 µA	1.464 µA	14.64 nA	1.464 nA	1.464 nA	488.2 pA	148.4 pA	14.84 pA
Total projected percent error	0.60%							

4.8 Physical properties

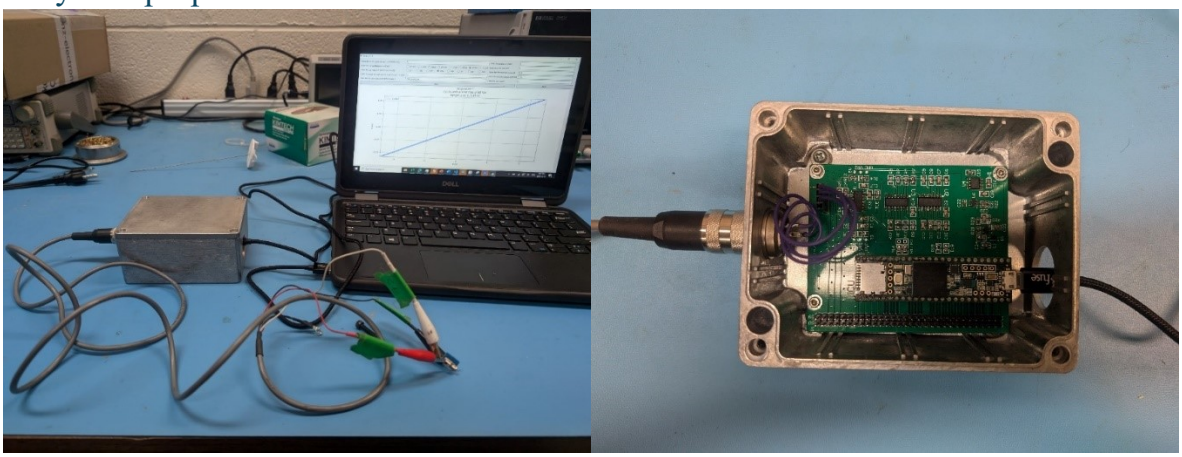

Figure 19: **CellStat** full system test with close-up

The **CellStat** is enclosed in an aluminum casing, which provides both mechanical protection and serves as a Faraday cage to shield against electromagnetic interference (EMI). The cables connecting to the working electrode (WE), reference electrode (RE), and counter electrode (CE) are shielded wires to further reduce noise and improve signal integrity. Additionally, both the aluminum casing and the cables are grounded to minimize EMI, ensuring stable and accurate measurements, particularly during sensitive electrochemical experiments.

A USB Micro-B port is used to transfer commands from the Teensy microcontroller to the computer and send the results back to the Python GUI. The computer must remain connected to the **CellStat** at all times to receive and process data. This direct connection ensures real-time data acquisition and control, which is critical for maintaining the functionality and accuracy of the potentiostat during experiments. These grounding and shielding measures, combined with the stable USB communication interface, ensure reliable performance in a variety of electrochemical applications.

4.8 Software design

The software controlling **CellStat** operates in two parts, using a structure adapted from the PassStat code. The computer software, written in Python, acts as the user interface (UI), allowing the operator to manage the potentiostat connection, send commands, and process data into Excel and text formats. The Python code is based on PassStat but was modified to integrate new functionality specific to **CellStat**. On the hardware side, the Teensy microcontroller code, written in C++, receives commands from the Python UI and executes electrochemical measurements, such as cyclic voltammetry (CV). While the base code was derived from the PassStat, significant changes were made to support the **CellStat**'s expanded features. These include adding MUX control for dynamic range selection and noise filtering, extending the voltage range to ±2.5V through DAC scaling, and adding functionality for battery charge and discharge testing over multiple scans. These modifications enable greater flexibility and precision in controlling the potentiostat. The initial testing with a 1 MΩ resistor shown in Fig. 21 verified system stability and validated the modified software.

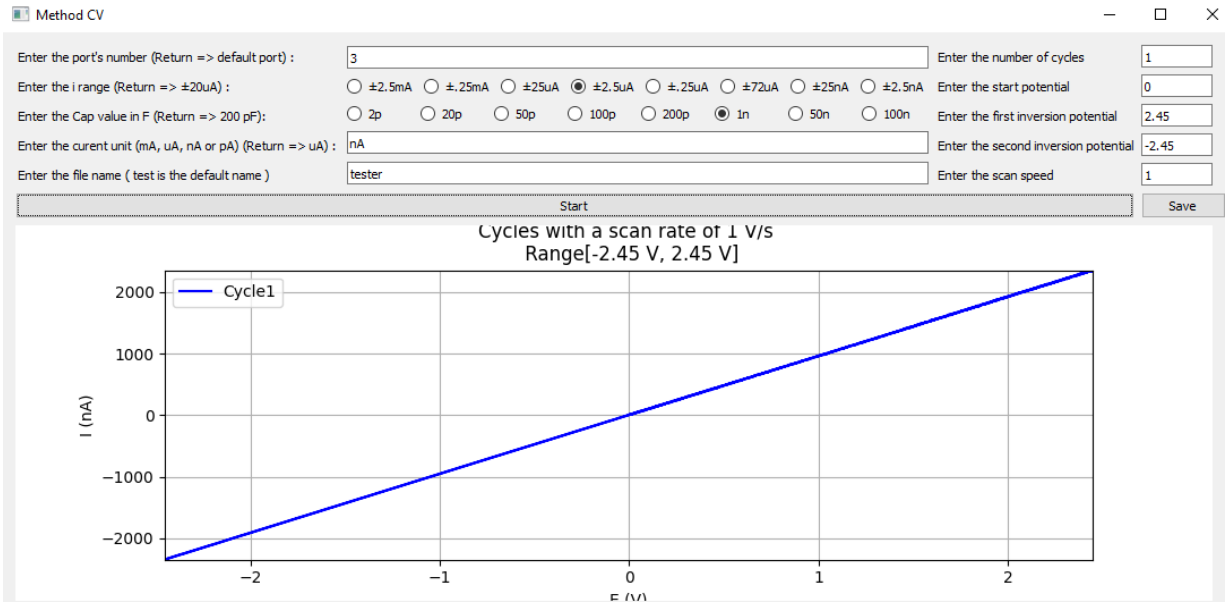

Figure 20: Initial testing of the potentiostat and software with a CV performed with a scan rate of 1 V/s over a potential range from -2.45 V to 2.45 V. The x-axis represents the potential (E) in volts, and the y-axis represents the current (I) in nanoamperes (nA).

Chapter 5: Validation of the Potentiostat

This chapter focuses on the validation of the **Cellstat** through a series of tests to better understand the overall performance. The validation process begins with the calibration of the potentiostats 16-bit ADC and DAC. This is followed by a compliance voltage test, which evaluates the potentiostats ability to maintain stable voltage levels. An accuracy test is also conducted to view the consistency and readings during electrochemical measurements. Additionally, a study is performed to assess how different scan rates might introduce bias into the collected data, examining the impact of these rates on the accuracy of the measurements.

5.1 Calibration

The calibration of **CellStat** was performed for each current range by comparing it with a test resistor placed between the WE and CE. This process ensures the accuracy of the measurements across different current ranges. The results presented in Fig. 25 and Fig.26 are the uncalibrated values. Calibration involves adjusting the potentiostat readings to match known values from the test resistor, compensating for any discrepancies of the offset and slope by the internal components, and changing the software calculations accordingly. The DAC calibration is done by applying a multimeter between the WE and CE and directly inputting bit values to measure the linear slope and offset of the DAC. This should be done before calibrating the ADC to ensure the offset of the ADC is not a function of the DAC offset.

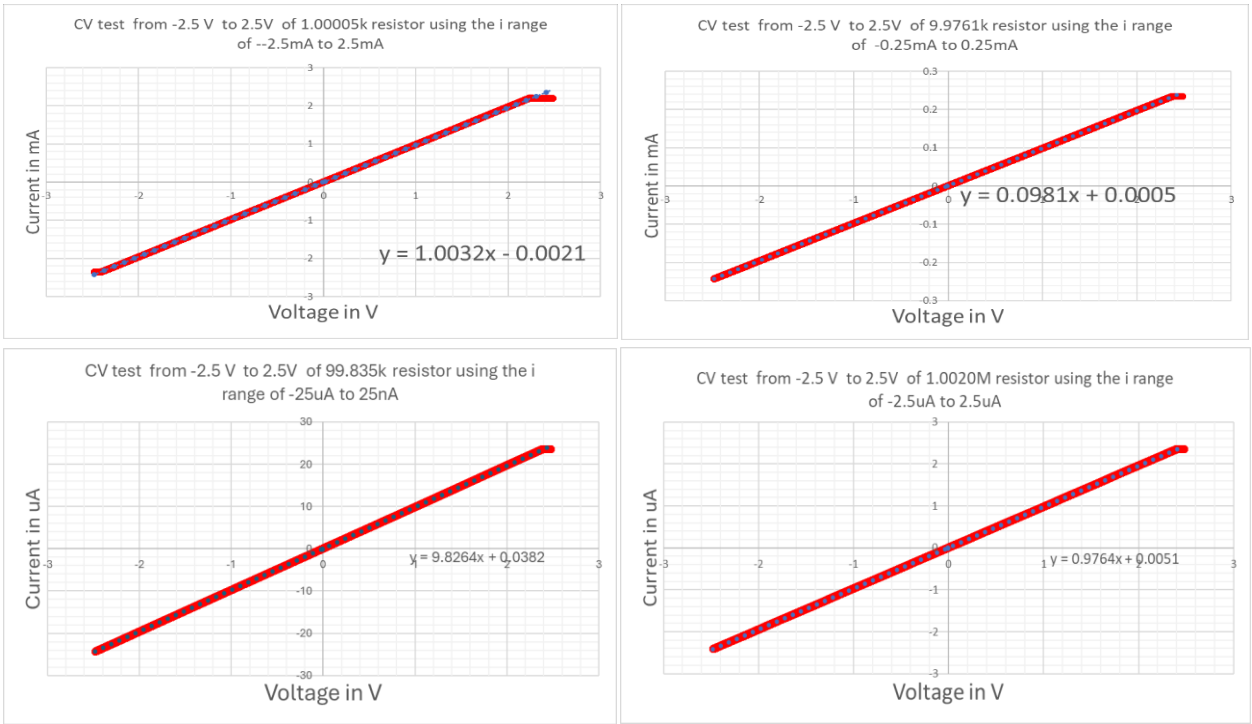

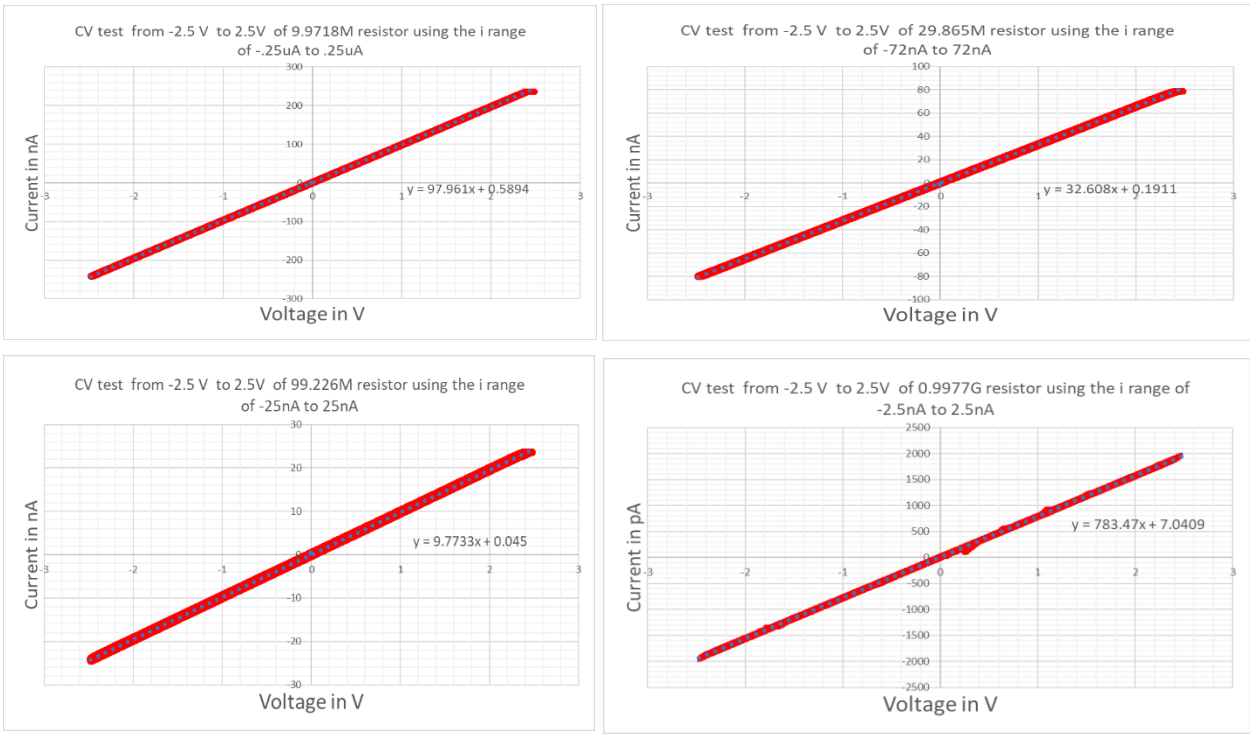

Figure 21: Calibration curve results of the ADC with external resistor

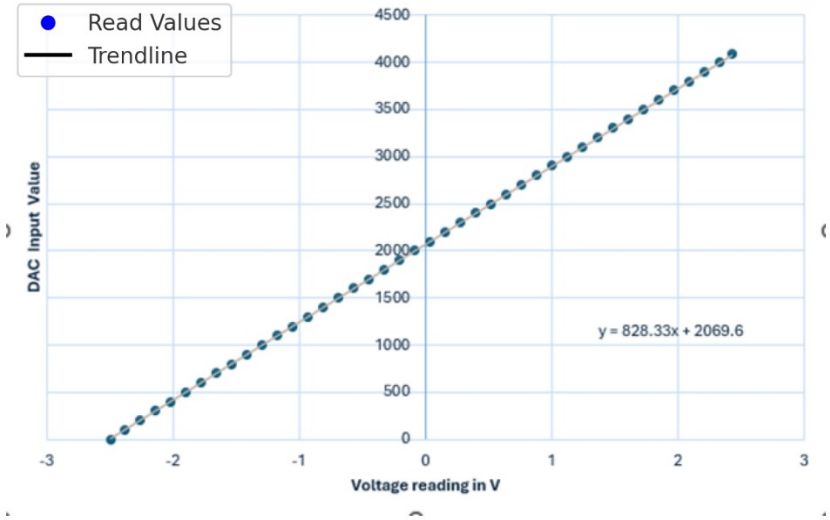

Figure 22: Plot of digitally set DAC values vs external measured voltage readings with a linear fit.

Table 6 summarizes the slopes, corresponding resistance values, and offset from the graphs. These values are used to calibrate the potentiostat by inputting them into the Python code of the GUI to

adjust the output values so that they match the expectations for the cell being tested. Each resistor used in the trans-impedance amplifier is tested to see the true value of the resistor and measure the slope of each resistor. The test was done at a scan speed of 1 V/s, the ideal filtering capacitor for this rate is to be 1 nF while for 1 G 0.2 nF is needed. The voltage step for the ADC is the voltage step per bit of the ADC adjusted for the slope difference found from the comparison of external resistance and the slope found. Refer to Appendix D for the process of adding these calibration values to the Cellstat code.

Table 6: Current calibration for each current range

Resistance index	Filtering Capacitor used (nF)	internal resistance value (kΩ)	External Resistance value (kΩ)	Slope measured (kΩ)	Percent slope offset	ADC offset in mV	ADC bit offset	offset ADC value	Adjusted voltage step (mV)
0	1	1	1.00005	1.0032	0.31%	-2.09	-2	2050	0.8084
1	1	10	9.9761	9.81	1.69%	5.10	4	2044	0.8195
2	1	100	99.835	98.264	1.60%	3.88	3	2045	0.8188
3	1	1000	1002	976.4	2.62%	5.22	4	2044	0.8270
4	1	10000	9971.8	9796.1	1.79%	6.02	5	2043	0.8203
5	1	30000	32608	29865	9.18%	5.86	5	2043	0.8798
6	1	100000	992260	977330	1.53%	4.60	4	2044	0.8182
7	.2	1000000	9977000	7834700	27.34%	8.92	7	2041	1.0262

The slopes of the 30MΩ and 1GΩ resistors show significant deviations from their expected values—9% for 30MΩ and 27% for 1GΩ. This discrepancy is probably primarily due to the inherent resistance of the PCB traces, leakage currents, and parasitic resistances throughout the circuit. The PCB itself has an overall board volume resistance in the range of 1GΩ. [39] This means that for extremely high-resistance measurements, a portion of the current is diffused through the board instead of being measured accurately by the circuit. This results in signal loss due to leakage through the traces, ICs, and wiring, leading to measurement errors at very high resistance values.

At lower resistance ranges, this effect is negligible because the dominant current path is through the intended circuit components. However, at higher resistance ranges, where currents are already in the picoamps range, even small leakage currents and PCB resistance variations become significant, distorting the expected measurement values. Understanding this deviation is critical because it directly affects the potentiostat's accuracy when working with high-impedance electrochemical cells. If uncorrected, these losses could introduce significant errors in experiments involving very low currents, such as nanoamp or picoamp-level measurements.

5.2 Voltage Offset

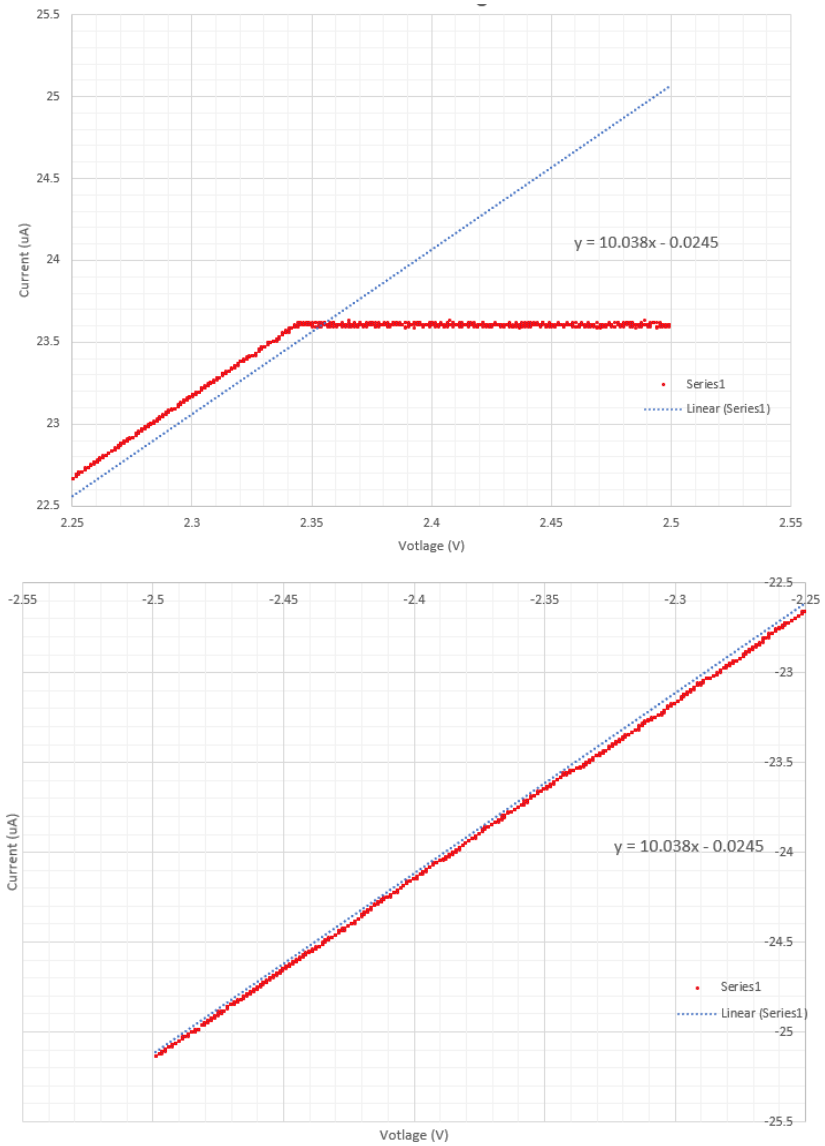

Figure 23: Zoomed in view of the voltage offset for the right edge (top) and left edge (bottom) for the 10 kΩ resistor with a linear trend line.

Fig. 23 is a zoomed-in view of a CV using a 10 kΩ resistor illustrating how the DAC calibration affects the potentiostat's voltage output. The relationship between applied voltage and measured current remains linear up to **2.4V**, as indicated by the linear fit. However, beyond **2.4V**, the current response begins to flatten, deviating from the expected trend. This deviation is due to the DAC calibration limits, which cause the output voltage to plateau rather than continue scaling proportionally. This is due to the adjusted DAC calibration for the adjusted offset and the adjusted slopes causing the overall range to be adjusted upwards. Thus, some voltage range is lost due to accuracy adjustments.

5.3 Linear deviation

The linear deviation analysis examines the performance of the potentiostat in terms of measurement consistency across various feedback resistors and current ranges. This section is critical in assessing how accurately the potentiostat measures current and voltage over a range of operational conditions.

Table 7: Precision comparisons by each feedback resistor at 1V/s

current range ±	2500 µA	250 µA	25000 nA	2500 nA	250 nA	83333 pA	25000 pA	2500 pA
standard deviation	10.29 µA	0.239 µA	24.68 nA	2.59 nA	0.87 nA	711.79 pA	272.33 pA	36.1 pA
mean error	8.22 µA	0.162 µA	17.32 nA	2.05 nA	0.71 nA	683.25 pA	237.93 pA	29.2 pA
max deviation	48.18 µA	0.751 µA	81.48 nA	8.72 nA	1.99 nA	1193.26 pA	533.85 pA	153.6 pA
percent deviation error	0.41%	0.10%	0.10%	0.10%	0.35%	0.85%	1.09%	1.45%
Percent mean error	0.33%	0.06%	0.07%	0.08%	0.28%	0.82%	0.95%	1.17%

Table 7 evaluates the measurement accuracy of the potentiostat across various feedback resistances after calibrating the current range. Specifically, it examines the deviation of measured values from an expected linear response based on Ohm's Law. The deviation is assessed through standard deviation, mean error, and maximum deviation. To quantify the deviation from linearity, a series of cyclic voltammetry (CV) scans were performed across different feedback resistances, with each measurement set consisting of three scans to ensure consistency and reproducibility. The analysis involves calculating the slope of the entire scan, determining the absolute error between measured values and the best-fit line, and quantifying the deviation using the root mean square deviation.

The results demonstrate that deviations remain minimal at lower feedback resistances, such as 1kΩ and 100kΩ, indicating high measurement accuracy in these conditions. However, as resistance increases, particularly above 30MΩ, deviations become more pronounced. This rise in deviation can primarily be attributed to the diminishing effectiveness of the feedback capacitor at higher resistances and lower current ranges. As a result, the system becomes more susceptible to external noise and interference, compromising the accuracy of the measurements.

Several factors influence this deviation. Firstly, the cutoff frequency response plays a significant role in measurement precision. During calibration, adjustments were made to maintain ideal filtering, using a 1nF capacitor across most feedback resistances. However, in scenarios involving high resistance, such as 1GΩ, a smaller 200 pF capacitor was employed to mitigate the increased deviation that arises due to the diminished effectiveness of the larger capacitor.[35] Secondly, electromagnetic interference becomes a considerable factor, particularly at lower current ranges, where the device is more vulnerable to external noise.

5.4 Accuracy deviation by scan rate

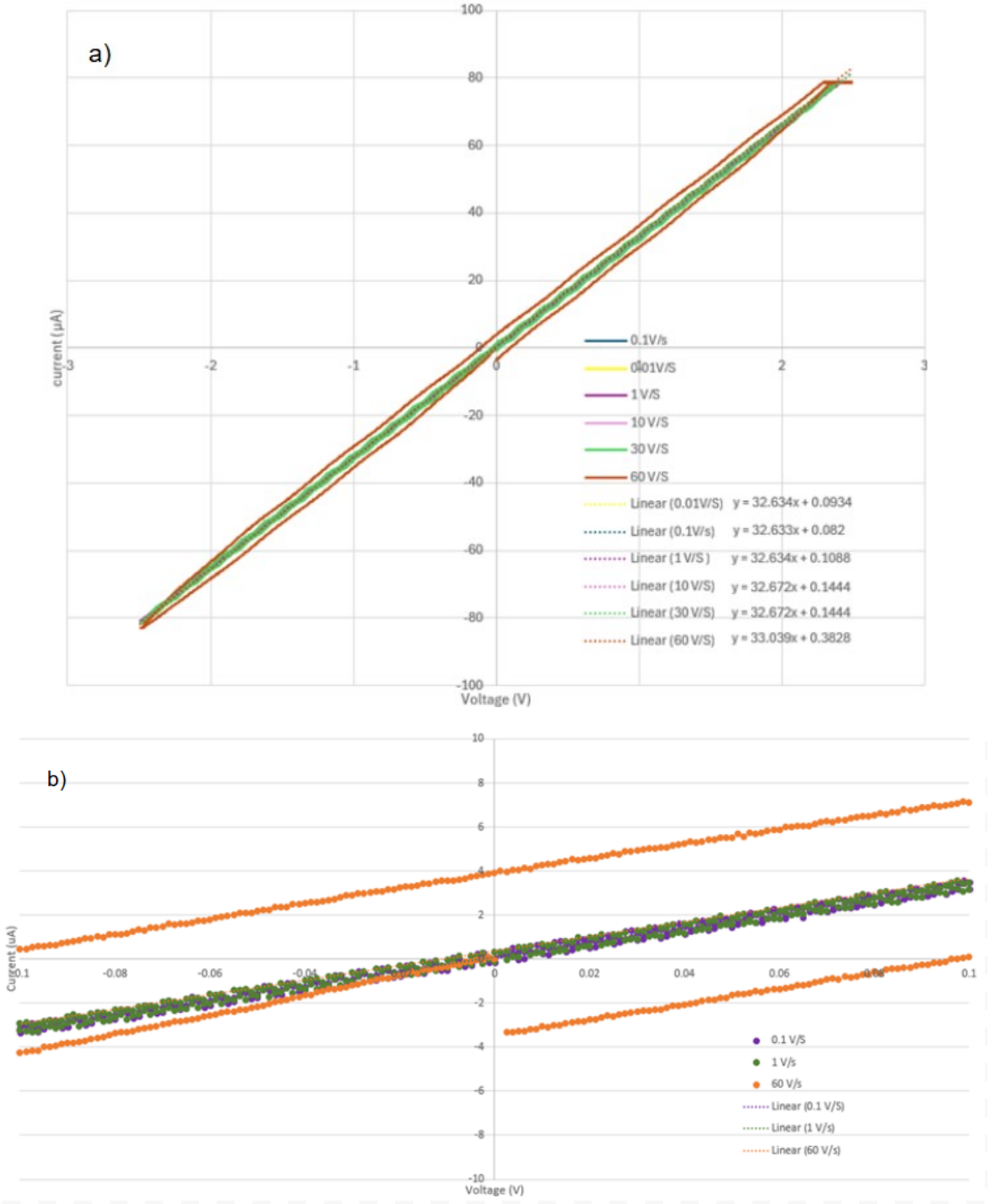

Figure 24: a) Voltage vs. Current Scatter Plot for Each Test b) Close-up of current vs. voltage readings with can speeds of 0.1V/s, 1V/s and 60V/s

A test was conducted to assess how different scan rates affect the CV response, as shown in Fig. 24. Using a 30 MΩ resistor, the slopes of the current-voltage graph were analyzed based on Ohm's Law ($V = I \times R$), where the slope should ideally reflect the resistor's value. However, deviations in slope at higher scan rates suggest the influence of impedance—which includes both resistance and capacitive effects—rather than pure resistance.

At higher scan rates, the CV curves showed rounding of the slope due to capacitive discharge during the scan. Additionally, the offset between the forward and backward scans became more pronounced at faster scan rates. At 60 V/s, this offset reached approximately 8 mA, indicating significant charge accumulation and discharge effects. The observed deviations and increasing offsets at higher scan rates highlight the impact of capacitive behavior and impedance, which must be considered when analyzing CV results at faster scan speeds.

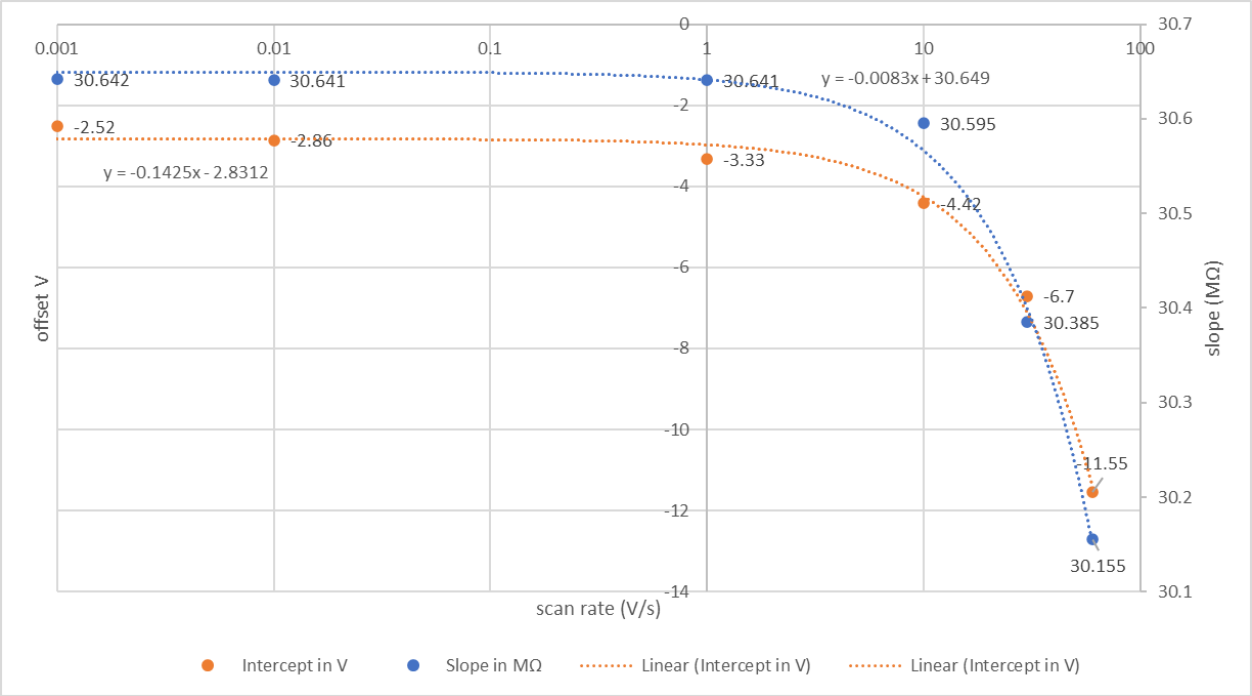

Figure 25: Deviation of slope and offset by scan rate.

Fig.25 explains how the DAC functions and highlights the need for calibration of current readings across different resistance ranges if absolute precision is required. The offset observed in the data arises from uncertainty in internal resistance, while changes in the slope are due to gain bias from the ICs.

Current leakage can be measured at different scan rates by analyzing the slopes for each scan rate. Fig.25 shows that the slopes, and thus the measured current, remain stable at lower scan speeds, making low scan rates preferable for applications requiring long-duration stability. However, as scan rates increase, deviations in the readings become more pronounced. This increase in deviation is due to capacitor discharge effects, which cause non-ideal behavior in the current response. The

capacitors within the system, particularly those used for noise filtering and stability, introduce transient charge storage that discharges more noticeably at higher scan rates, leading to the observed curvature in the data.

This explains the curvature previously mentioned in Section 5.3, where the response deviates from an ideal linear relationship. The discharge effect becomes more significant at higher scan rates, affecting measurement accuracy. Understanding this behavior is essential for optimizing the potentiostat's performance, particularly for experiments requiring high-speed data acquisition.

5.5 Effects of filtering

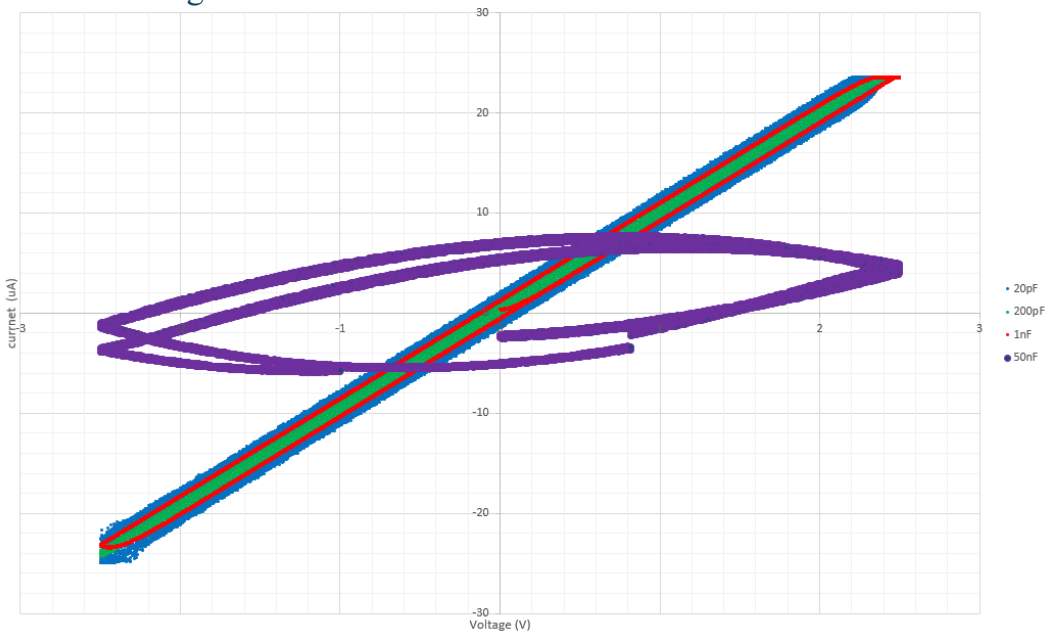

Figure 26: Demonstration of the capacitor filtering of 100M resistor at 1 V/s

Fig.26 demonstrates the effect of different capacitor values on the filtering system at a scan rate of 1 V/s, showing how the choice of capacitor impacts the quality of the electrochemical measurement. The plotted data represent CV responses using various capacitors in the RC filtering system of the potentiostat.

The results show that when using low-capacitance values such as 20 pF, significant noise is present in the measurement. This occurs because insufficient filtering allows high-frequency components and external interference to distort the signal, leading to an unstable and scattered response. In contrast, a 200 pF capacitor provides an optimal balance, effectively filtering out noise while maintaining a clean, linear CV curve. This suggests that 200 pF is the ideal filtering capacitor for this specific test setup, as it preserves signal integrity without excessive distortion. When using larger capacitance values such as 1 nF and 50 nF, the response becomes increasingly distorted due to capacitor discharge effects. Excessive capacitance slows the response time of the system, causing the measured current to lag behind the applied voltage, leading to curvature and looping in the CV trace.

These results emphasize the importance of selecting an appropriate capacitor value in the **CellStat** RC filter. If the capacitance is too low, excessive noise degrades measurement accuracy, whereas if the capacitance is too high, capacitor discharge effects introduce distortion and time lag. The optimal capacitor value depends on the current range and scan rate used in the experiment, meaning that capacitor selection must be determined on a case-by-case basis to achieve the best filtering performance for a given electrochemical system. A preliminary test and best guess are necessary, to find the best capacitor and then choose the one that gives the best data. For general use, the 1nF capacitor is good for all tests that are less than 1 V/s but for higher or using the 1GΩ use a lower value capacitor.[35]

Chapter 6: Experimental Testing with Flow Battery Electrolytes

This chapter focuses on conducting a series of electrochemical tests using a well-known redox couple, ferro/ferricyanide, commonly applied in electrochemical studies. The goal is to evaluate the performance and accuracy of the developed potentiostat by comparing its results to those obtained from a commercial benchmark device, the Lab Biologic system. This comparative analysis will highlight the potentiostat's capability in handling real-world electrochemical testing scenarios and determine its potential as a cost-effective alternative for laboratory research and practical applications.

6.1 Introduction to Experimental Testing

In this section, we present a series of electrochemical tests designed to evaluate the performance of the developed potentiostat under varying concentrations and SOC conditions. A total of six tests were conducted, divided between 0.1 M FeCN and 0.01 M FeCN solutions. In shorthand, we refer to these as "0.1 M FeCN" or "0.01 M FeCN," but in practice, these solutions contained a defined ratio of ferrocyanide ($[Fe(CN)_6]^{4-}$) and ferricyanide ($[Fe(CN)_6]^{3-}$), with potassium hydroxide (KOH) as the supporting electrolyte.

To properly account for changes in oxidation states relevant to battery and redox-flow applications in microelectrode systems, SOC levels were adjusted differently depending on the solution composition. At 50% SOC, the ferrocyanide and ferricyanide concentrations were equal. However, at 10% and 90% SOC, the ratio of the two species was adjusted accordingly to reflect a predominantly reduced or oxidized state, respectively. These adjustments ensured that the potentiostat was tested under realistic operating conditions and that the measured electrochemical behavior accurately represented the system's response across different oxidation states.

6.2 Methodology

The following materials were prepared in a three-electrode stagnant cell configuration. CVs were conducted using the commercial Biologic potentiostat first, followed by measuring the CV with the same settings using the CellStat. All CVs were recorded at 1mV/s scan rate.

- Samples :
    1. 0.1M FeCN in 1M potassium chloride at 10%, 50% and 90% SOC
    2. 0.01M FeCN in 1M potassium chloride at 10%, 50% and 90% SOC
- Electrodes Used:
    1. Working Electrode: Graphite rod
    2. Reference Electrode: Silver chloride (Ag/AgCl) electrode
    3. Counter Electrode: Platinum wire

6.3 Experimental Testing results

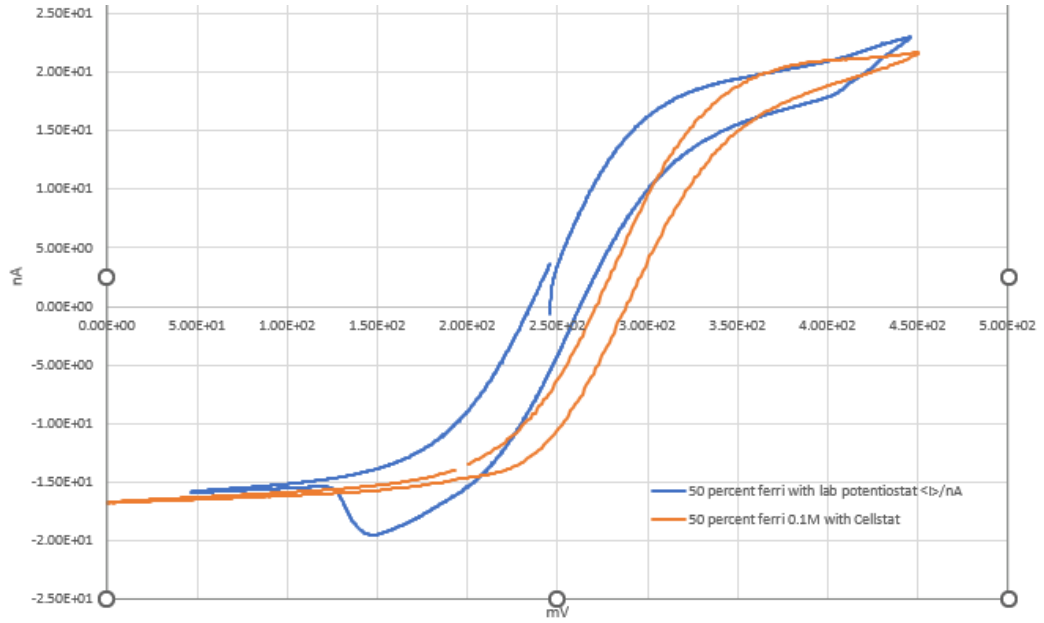

Figure 27: CV at 1 mV/s for a 0.1M FeCN solution at 50% SOC

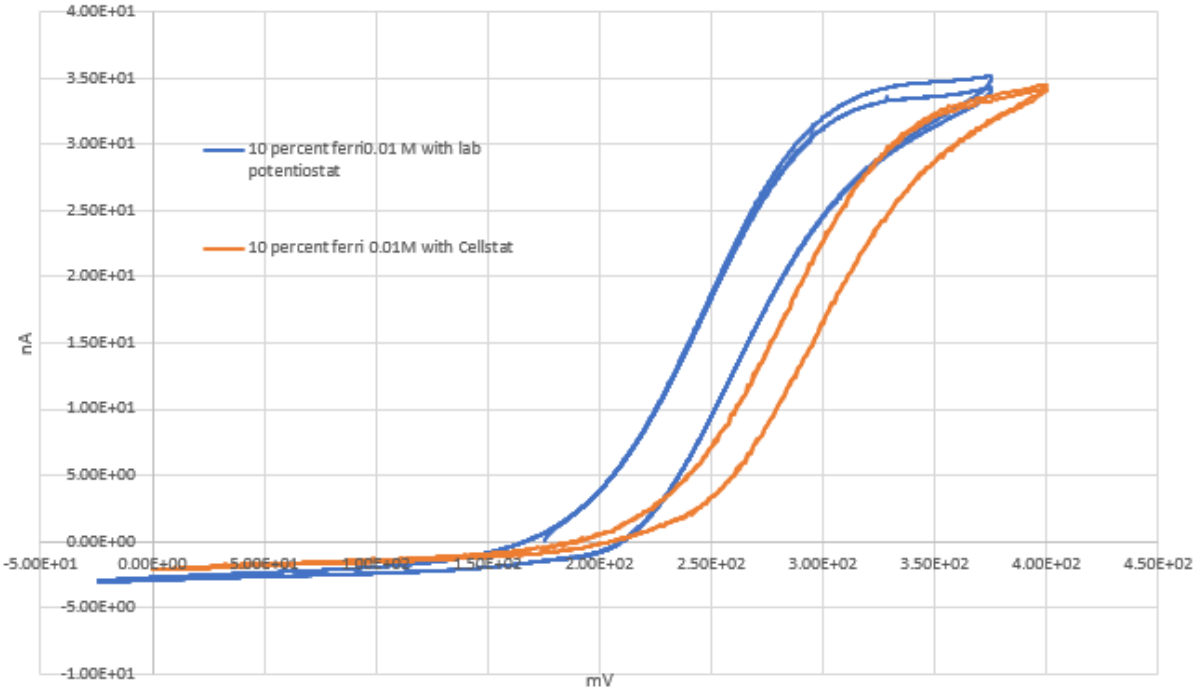

Figure 28: CV at 1 mV/s for a 0.1M FeCN solution at 10% SOC

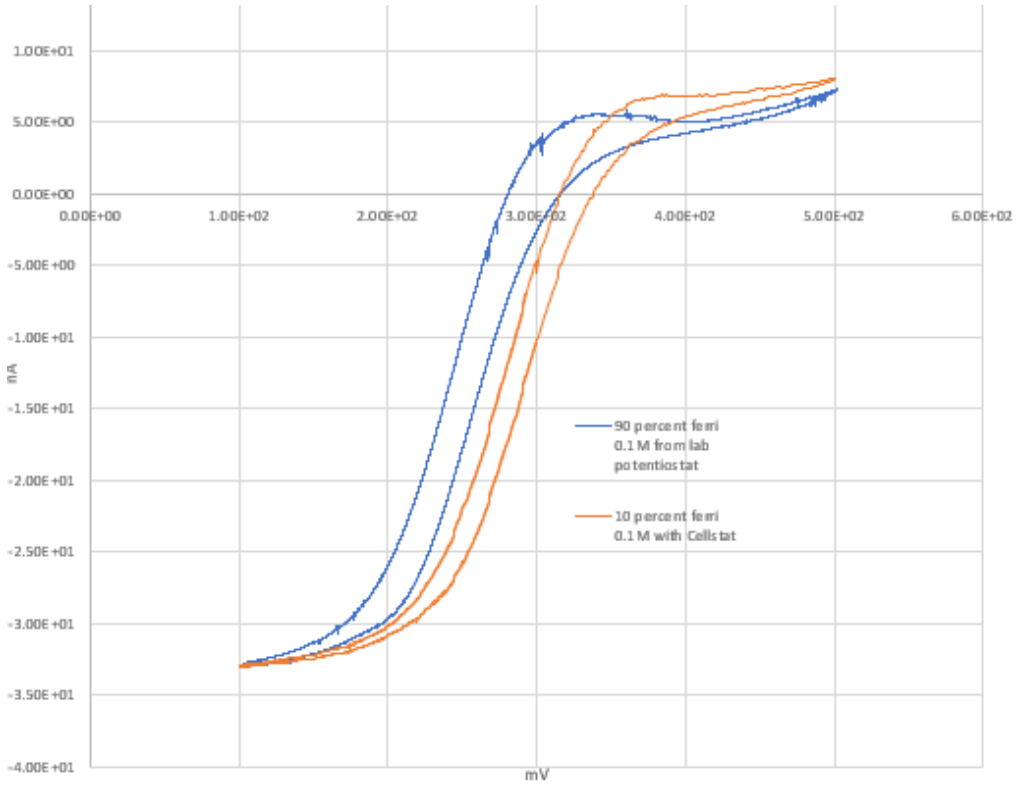

Figure 29: CV at 1 mV/s for a 0.1M FeCN solution at 90% SOC

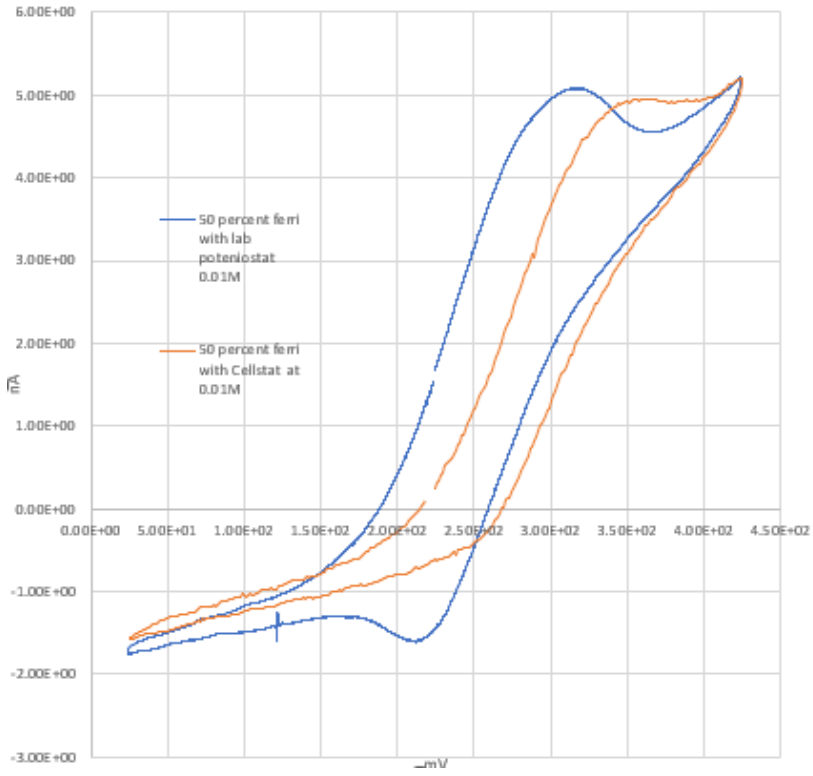

Figure 30: CV at 1 mV/s for a 0.01M FeCN solution at 50% SOC

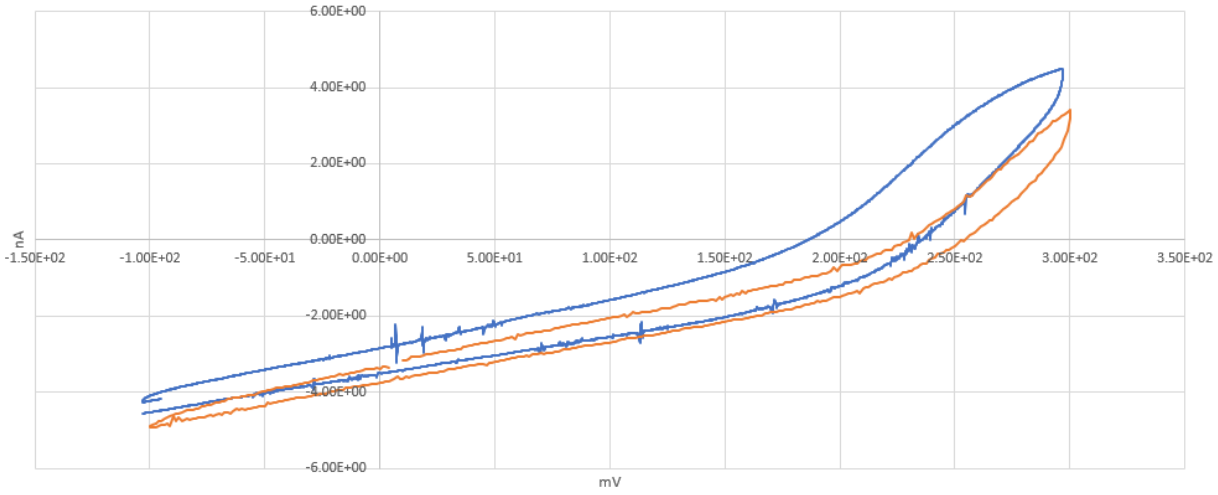

Figure 31: CV at 1 mV/s for a 0.01M FeCN solution at 90% SOC

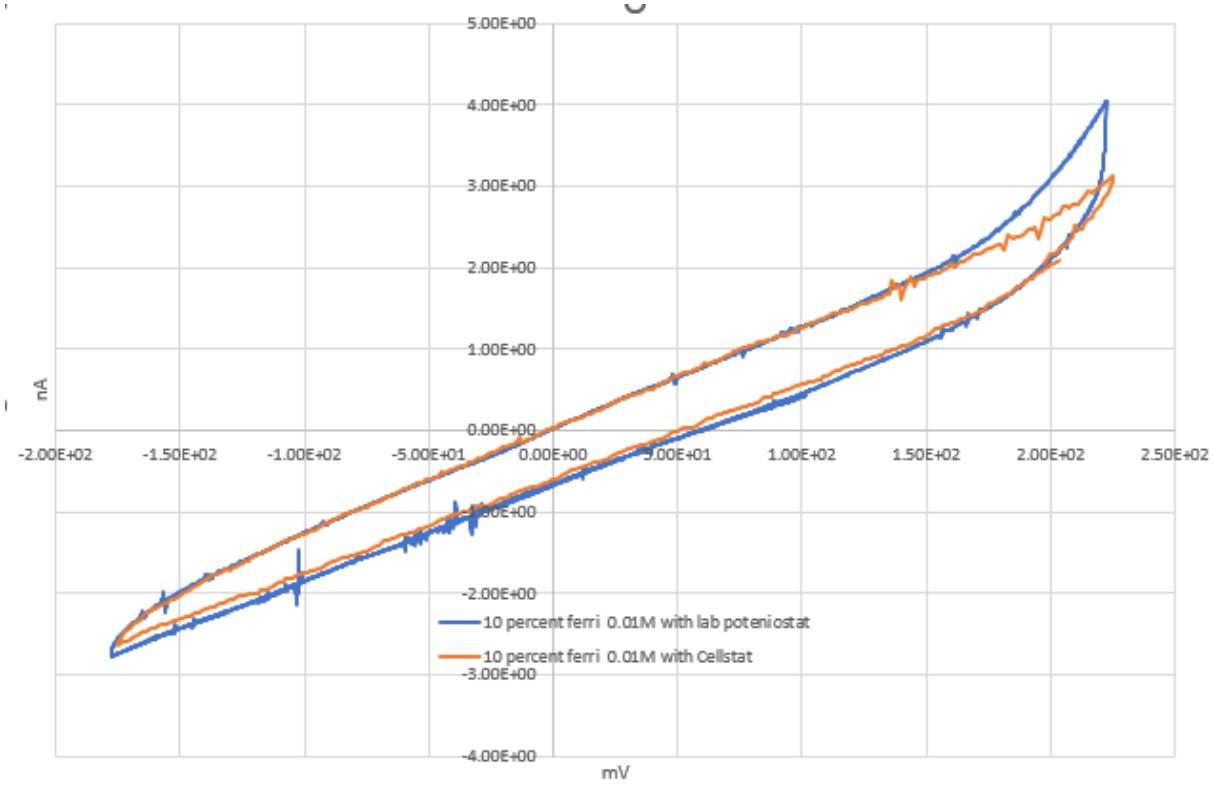

Figure 32: CV at 1 mV/s for a 0.01M FeCN solution at 10% SOC

The results from the experimental testing show that the cyclic voltammetry (CV) curves obtained from both the Lab Biologic system and the CellStat potentiostat generally follow the same overall curvature, indicating consistent electrochemical behavior across both devices. However, some deviations were observed between the two systems.

In many cases, the curves for the CellStat data are shifted to more positive potentials. This is because the scans were performed right after those with the Biologic, which resulted in a shift in the OCV of the solution.

Other deviations can likely be attributed to the proprietary data processing methods used by the Lab Biologic system, as its closed-source nature leaves the specifics of its data acquisition and processing methods unclear. Additionally, the CV curves from the Lab Biologic system displayed unaccounted capacitances and occasional signal spikes, which could contribute to irregularities in the data. In contrast, the CellStat potentiostat produced smoother and more consistent curves, staying within the expected range for accurate electrochemical readings. Based on these findings, the CellStat demonstrates reliable performance, providing results that align closely with standard electrochemical behavior, thereby validating its effectiveness as a dependable and cost-efficient testing tool.

Chapter 7: Conclusions and Future Work

7.1 Conclusions

The CellStat potentiostat has been developed to meet the laboratory's guidelines and requirements, offering a user-friendly interface with high current precision. The system's accuracy relies on proper calibration between the DAC and all eight feedback resistors to the ADC, ensuring reliable electrochemical measurements. Additionally, frequency filtering is controlled based on scan rate, feedback resistors, and feedback capacitor selection, all of which influence measurement accuracy and quality. While the overall accuracy deviation remains below 3%, deviations increase significantly at lower current ranges, particularly at 2 nA. This increase in error is primarily due to the impact of electromagnetic interference, which introduces noise into the system at such low currents. To mitigate this, electromagnetic shielding techniques—such as proper grounding and optimized feedback capacitor selection—should be implemented. Despite these challenges, the CellStat successfully provides reliable state-of-charge (SOC) and state-of-health (SOH) assessments for flow battery testing.

7.2 Long term goals

After the preliminary testing mentioned in section 6 and discussions about future implementation, some design improvements were identified that would be beneficial for the next version of the CellStat. Future improvements can be categorized into two main areas: those requiring a new PCB design and those that can be addressed without redesigning the PCB.

7.2.1 Ideas for PCB improvements

- Teensy 4.1 Integration: The current CellStat design is based on the Teensy 3.6, which has been discontinued. The Teensy 4.1 lacks a built-in DAC, requiring an external DAC for compatibility. A new PCB layout will be necessary to accommodate this change.
- Impedance Measurements: Incorporating impedance spectroscopy capabilities would expand the system's functionality for electrochemical analysis. This would require additional circuitry for AC signal injection and response measurement.
- Wireless Communication (Bluetooth/Wi-Fi): Adding a Bluetooth or Wi-Fi module would allow for remote data acquisition and control, improving usability in distributed testing environments.

7.2.2 Ideas for external improvements

- Casing and Shielding: The aluminum enclosure provides some electromagnetic shielding but is not sealed against harsh chemical environments. Improved sealing around the USB and connection cables would enhance durability. Additionally, grounding the metal enclosure or incorporating a Faraday cage design would further reduce electromagnetic noise.
- Software and User Interface: The current software, based on the PassStat framework, can be enhanced by refining the Python code to support additional test parameters and new experimental techniques. A more robust communication protocol and optimized data processing framework would improve reliability and ease of use.

- Noise Reduction Practices: Implementing better grounding techniques, such as via stitching and chassis grounding, will help minimize electromagnetic interference in the current design.

References

[1] Y. Ma, P. Yang, X. Zhou, and Z. Gao, “Research review on energy storage technology,” in *2016 IEEE International Conference on Mechatronics and Automation*, Aug. 2016, pp. 159–164. doi: 10.1109/ICMA.2016.7558553.

[2] T. Jun, “Energy storage technology in the application of distributed generation,” *Power Systems Engineering*, vol. 4, no. 8, pp. 28–42, 2010.

[3] C. Zhou and T. Li, “Research on Liquid Metal Energy Storage Battery Equalization Management System in Power PSS,” *Procedia CIRP*, vol. 83, pp. 547–551, Jan. 2019, doi: 10.1016/j.procir.2019.04.117.

[4] H. Kim *et al.*, “Liquid Metal Batteries: Past, Present, and Future,” *Chem. Rev.*, vol. 113, no. 3, pp. 2075–2099, Mar. 2013, doi: 10.1021/cr300205k.

[5] W. Wang, Q. Luo, B. Li, X. Wei, L. Li, and Z. Yang, “Recent progress in redox flow battery research and development,” *Adv. Funct. Mater.*, vol. 23, no. 8, pp. 970–986, Feb. 2013, doi: 10.1002/adfm.201200694.

[6] O. Nolte, I. A. Volodin, C. Stolze, M. D. Hager, and U. S. Schubert, “Trust is good, control is better: a review on monitoring and characterization techniques for flow battery electrolytes,” *Mater. Horiz.*, vol. 8, no. 7, pp. 1866–1925, 2021, doi: 10.1039/D0MH01632B.

[7] Y. Ashraf Gandomi *et al* “Critical Review—Experimental Diagnostics and Material Characterization Techniques Used on Redox Flow Batteries" J. Electrochem. Soc, vol 165 , pp. A970, 2018, doi: 10.1149/2.0601805jes [8] K. Gong, Q. Fang, S. Gu, S. F. Y. Li, and Y. Yan, “Nonaqueous redox-flow batteries: organic solvents, supporting electrolytes, and redox pairs,” *Energy Environ. Sci.*, vol. 8, no. 12, pp. 3515–3530, Nov. 2015, doi: 10.1039/C5EE02341F.

[9] Y. Wang, H. Liu, Z. Jia, B. Yang, and L. He, “The Electrochemical Performance of Al-Mg-Ga-Sn-xBi Alloy Used as the Anodic Material for Al-Air Battery in KOH Electrolytes,” *Crystals*, vol. 12, p. 1785, Dec. 2022, doi: 10.3390/cryst12121785.

[10] N. Elgrishi, K. J. Rountree, B. D. McCarthy, E. S. Rountree, T. T. Eisenhart, and J. L. Dempsey, “A Practical Beginner’s Guide to Cyclic Voltammetry,” *J. Chem. Educ.*, vol. 95, no. 2, pp. 197–206, Feb. 2018, doi: 10.1021/acs.jchemed.7b00361.

[11] Quang-Dao Trinh “Cyclic Voltammetry: Characteristic Points - Wolfram Demonstrations Project.” Accessed: Jun. 07, 2024. [Online]. Available: https://demonstrations.wolfram.com/CyclicVoltammetryCharacteristicPoints/

[12] C. Bracher et al“Cyclic Voltammetry Basic Principles, Theory & Setup,” Ossila.com. Accessed: Aug. 08, 2024. [Online]. Available: https://www.ossila.com/pages/cyclic-voltammetry

[13] ROHM Semiconductor, “Opamp Comparator:What are Opamps and Comparators?" Electronics Basics ROHM.” Accessed: Aug. 08, 2024. [Online]. Available: https://www.rohm.com/electronics-basics/opamps/what-are-opamps-comparators

[14] EEE guide, “Voltage Follower Op Amp | Advantages of Voltage Follower,” EEEGUIDE.COM. Accessed: Aug. 09, 2024. [Online]. Available: https://www.eeeguide.com/voltage-follower-op-amp/

[15] Pine Research, “A practical guide to choosing a potentiostat,” Pine Research. Accessed: Oct. 25, 2024. [Online]. Available: https://pineresearch.com/blog/practical-choosing-potentiostat/

[16] Dr.Bob, “Potentiostat Compliance Voltage,” Electrochemistry Resources. Accessed: Oct. 25, 2024. [Online]. Available: https://electrochemistryresources.com/potentiostat-compliance-voltage/

[17]D. Snizhko, Y. Zholudov, A. Kukoba, and G. Xu, “Potentiostat design keys for analytical applications,” *J. Electroanal. Chem.*, vol. 936, p. 117380, May 2023, doi: 10.1016/j.jelechem.2023.117380.
[18]PalmSens, “Sensit Smart,” PalmSens. Accessed: Aug. 20, 2024. [Online]. Available: https://www.palmsens.com/product/sensit-smart/
[19]PalmSens, “PalmSens4,” PalmSens. Accessed: Jun. 10, 2024. [Online]. Available: https://www.palmsens.com/product/palmsens4/
[20]Metrohm, “µStat-i 400 Bipotentiostat/Galvanostat/Impedance Analyzer (EIS).” Accessed: Aug. 20, 2024. [Online]. Available: https://www.metrohm.com/en/products/s/tat-/stat-i-400.html
[21]Corrtest Instruments,“Portable potentiostat CS100E (with EIS)-Corrtest Instruments.” Accessed: Aug. 20, 2024. [Online]. Available: https://www.corrtest.com.cn/en/extendedseries/1396.html
[22]A. Hill, S. Tait, P. Harris, C. Baillie, B. Virdis, and B. K. McCabe, “Design and analysis of a low-cost potentiostat for application with microbial electrochemical sensors,” *Electrochimica Acta*, vol. 468, p. 143201, Nov. 2023, doi: 10.1016/j.electacta.2023.143201.
[23]A. Ainla *et al.*, “Open-Source Potentiostat for Wireless Electrochemical Detection with Smartphones,” *Anal. Chem.*, vol. 90, no. 10, pp. 6240–6246, May 2018, doi: 10.1021/acs.analchem.8b00850.
[24]M. D. M. Dryden and A. R. Wheeler, “DStat: A Versatile, Open-Source Potentiostat for Electroanalysis and Integration,” *PLOS ONE*, vol. 10, no. 10, p. e0140349, Oct. 2015, doi: 10.1371/journal.pone.0140349.
[25]A. A. Rowe *et al.*, “CheapStat: An Open-Source, ‘Do-It-Yourself’ Potentiostat for Analytical and Educational Applications,” *PLOS ONE*, vol. 6, no. 9, p. e23783, Sep. 2011, doi: 10.1371/journal.pone.0023783.
[26]A. Scott, R. Pandey, S. Saxena, E. Osman, Y. Li, and L. Soleymani, “A Smartphone Operated Electrochemical Reader and Actuator that Streamlines the Operation of Electrochemical Biosensors,” *ECS Sens. Plus*, vol. 1, no. 1, p. 014601, Apr. 2022, doi: 10.1149/2754-2726/ac5fb3.
[27]M. W. Glasscott, M. D. Verber, J. R. Hall, A. D. Pendergast, C. J. McKinney, and J. E. Dick, “SweepStat: A Build-It-Yourself, Two-Electrode Potentiostat for Macroelectrode and Ultramicroelectrode Studies,” *J. Chem. Educ.*, vol. 97, no. 1, pp. 265–270, Jan. 2020, doi: 10.1021/acs.jchemed.9b00893.
[28]O. S. Hoilett, J. F. Walker, B. M. Balash, N. J. Jaras, S. Boppana, and J. C. Linnes, “KickStat: A Coin-Sized Potentiostat for High-Resolution Electrochemical Analysis,” *Sensors*, vol. 20, no. 8, Art. no. 8, Jan. 2020, doi: 10.3390/s20082407.
[29]P. Irving, R. Cecil, and M. Z. Yates, “MYSTAT: A compact potentiostat/galvanostat for general electrochemistry measurements,” *HardwareX*, vol. 9, p. e00163, Apr. 2021, doi: 10.1016/j.ohx.2020.e00163.
[30]T. Dobbelaere, P. M. Vereecken, and C. Detavernier, “A USB-controlled potentiostat/galvanostat for thin-film battery characterization,” *HardwareX*, vol. 2, pp. 34–49, Oct. 2017, doi: 10.1016/j.ohx.2017.08.001.
[31]D. M. Jenkins, B. E. Lee, S. Jun, J. Reyes-De-Corcuera, and E. S. McLamore, “ABE-Stat, a Fully Open-Source and Versatile Wireless Potentiostat Project Including Electrochemical Impedance Spectroscopy,” *J. Electrochem. Soc.*, vol. 166, no. 9, p. B3056, Mar. 2019, doi: 10.1149/2.0061909jes.

[32]P. Lopin and K. V. Lopin, “PSoC-Stat: A single chip open source potentiostat based on a Programmable System on a Chip,” *PLOS ONE*, vol. 13, no. 7, p. e0201353, Jul. 2018, doi: 10.1371/journal.pone.0201353.
[33]S. Sarkar and M. Bhattacharya, "SStat: Wi-Fi and Bluetooth integrated Multimodal "Do-It-Yourself" Electrochemical Potentiostat," *IECON 2020 The 46th Annual Conference of the IEEE Industrial Electronics Society*, Singapore, 2020, pp. 5249-5254, doi: 10.1109/IECON43393.2020.9254701.
[34]IO Rodeo, “Rodeostat: open source potentiostat,” IO Rodeo. Accessed: Aug. 21, 2024. [Online]. Available: https://iorodeo.com/products/rodeostat
[35]M. Caux *et al.*, “PassStat, a simple but fast, precise and versatile open source potentiostat,” *HardwareX*, vol. 11, p. e00290, Apr. 2022, doi: 10.1016/j.ohx.2022.e00290.
[36]G. N. Meloni, “Building a Microcontroller Based Potentiostat: An Inexpensive and Versatile Platform for Teaching Electrochemistry and Instrumentation,” *J. Chem. Educ.*, vol. 93, no. 7, pp. 1320–1322, Jul. 2016, doi: 10.1021/acs.jchemed.5b00961.
[37]Y. C. Li *et al.*, “An Easily Fabricated Low-Cost Potentiostat Coupled with User-Friendly Software for Introducing Students to Electrochemical Reactions and Electroanalytical Techniques,” *J. Chem. Educ.*, vol. 95, no. 9, pp. 1658–1661, Sep. 2018, doi: 10.1021/acs.jchemed.8b00340.
[38]MaxLinear,“SPX5205”.Maxlinear.com Accessed: Feb. 23, 2025 [Online]. https://www.maxlinear.com/product/power-management/power-conversion/ldos-and-regulators/linear-regulators-ldos/spx5205
[39]MADPCB, “Surface Resistivity (ρS) - Property of Printed Circuit Board (PCB) Materials" MADPCB. Accessed: Feb. 23, 2025. [Online]. Available: https://madpcb.com/glossary/surface-resistivity/

Appendix

Appendix A: PCB diagram

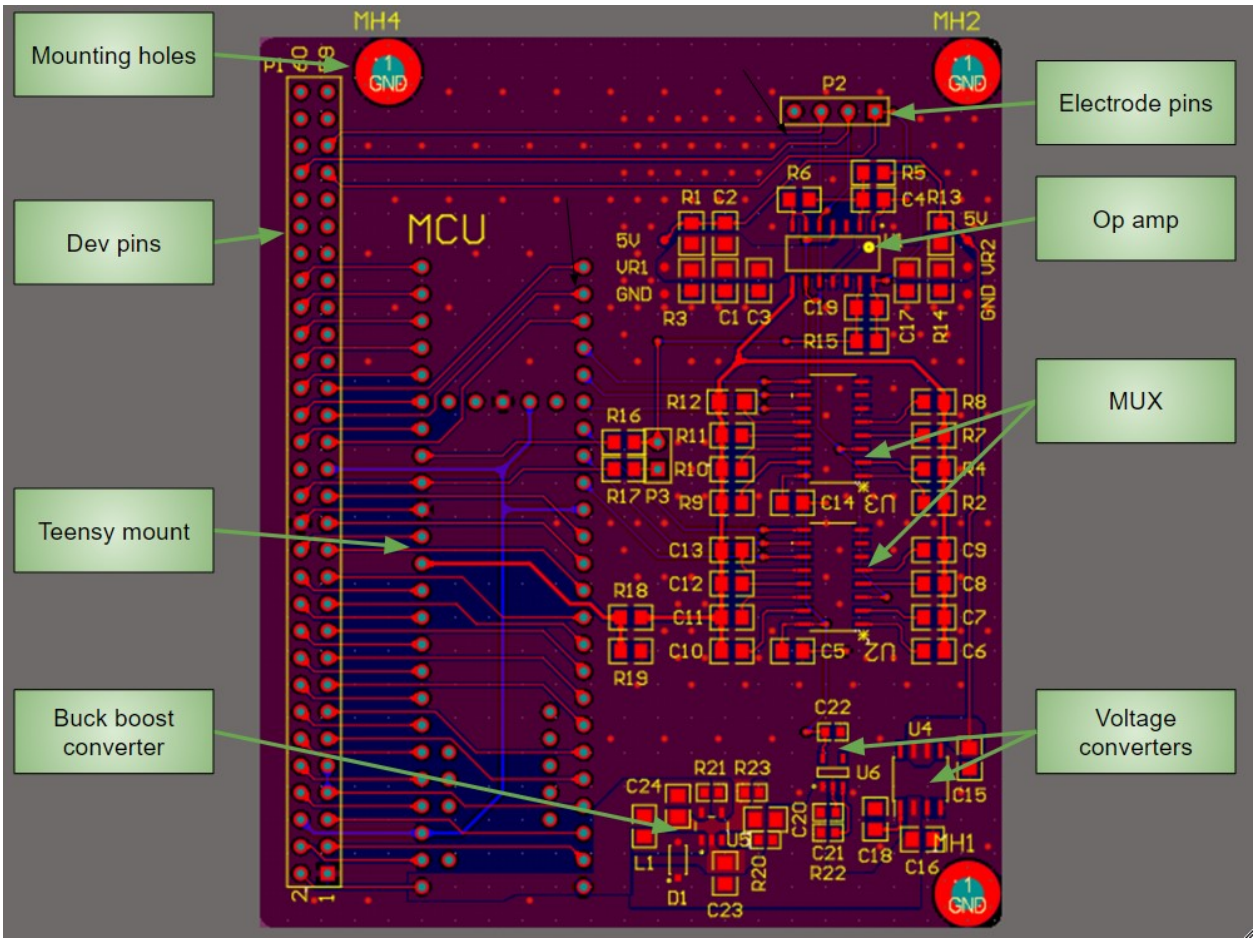

Figure 32: Gerber files of the new potentiostat

Appendix B: Method of getting ideal filtering capacitor

This section explains the different settings and inputs for using a cyclic voltammetry (CV) potentiostat. shows the software used to make the reading, how to set up the port number, current range, capacitance value, potential inversion points, and scan speed. Understanding these settings is important for getting accurate measurements. Also explaining how to calculate the sampling rate and the importance of initial testing with resistors to ensure the system works correctly.

1. Enter the port's number: This field is used to specify the serial port number that the potentiostat is connected to. The port number is based on the USB port that the computer is connected to the potentiostat. It allows communication between the software and the hardware.
2. Enter the i range: This selection allows you to set the current range for the measurements. The options include ±2.5mA, ±.25mA, ±25µA, ±2.5µA, ±.25µA, ±72nA, ±25nA, and ±2.5nA. Choosing the appropriate range ensures accurate measurement of current.
3. Enter the Capacitance value in F: This option sets the capacitance value in Farads. The options range from 2pF to 100nF. Choosing the appropriate capacitance value is based on the formula

   $$f_{cf} = \frac{1}{2\pi RfCf}$$

   This setting is important for configuring the compensation for the system's inherent capacitance. The cut-off frequency needs to be just higher than the frequency of the sample rate, which is calculated using the formula:

   $$sampling\ rate(Hz) = \frac{scan\ rate\left(\frac{V}{s}\right)}{potenital\ step\ size(V)}$$

   with the potential step size being 1.22 mV.

4. Enter the current unit: You can select the unit for measuring current, which can be mA (milliampere), µA (microampere), nA (nanoampere), or pA (picoampere). This ensures the data is displayed in the desired unit of measure.
5. Enter the number of cycles: This field allows you to specify how many CV cycles you want to run. The number of cycles must be a value between 1 and 3. A cycle involves sweeping the potential from a starting value to an inversion point and then back.
6. Enter the start potential: This sets the initial potential value for the CV scan. The Start potential must be a value between the second and third inversion values.

7. Enter the first inversion potential: This is the potential at which the scan direction will invert for the first time. The inversion potentials must be a value between -2.5 and 2.5 V.
8. Enter the second inversion potential: This is the potential at which the scan direction will invert for the second time.

9. Enter the scan speed: This determines the rate at which the potential is swept during the CV scan, measured in volts per second (V/s).
10. Enter the file name: Here, you can specify the name of the file where the data will be saved. If no name is given, "test" is used as the default.
11. In the plot displayed, the x-axis represents the potential (E) in volts, and the y-axis represents the current (I) in nanoamperes (nA). The title of the graph indicates that the scan rate is 1 V/s, with a potential range from -2.45 V to 2.45 V.

Appendix C: Cutoff frequency calculations

Table 8: Full table of CellStats cut-off frequencies

Compliance Voltage ±V	2.5							
Resistor Values in kΩ	1	10	100	1000	10000	30000	100000	1000000
DAC/ADC Resolution	4096							
DAC Resolution mV	1.22							
DAC Bit Error (lSB) ±	8							
DAC Percent Error	0.20%							
DAC Error ±	9.76 µA	0.96 µA	97.68 nA	9.76 nA	0.976 nA	325.52 pA	97.68 pA	9.76 pA
ADC Range per Resistor ±	2.5 mA	0.25 mA	25 µA	2.5 µA	0.25 µA	83.33 nA	25 nA	2.5 nA
ADC Resolution	1.22 µA	0.12 µA	12.21 nA	1.22 nA	0.122 nA	40.69 pA	12.21 pA	1.22 pA
ADC Bit Error (lSB) ±	4							
ADC Error ±	39.04 µA	3.904 µA	390.4 nA	39.04 nA	3.904 nA	1302.08 pA	390.4 pA	39.04 pA
Cutoff Frequency for 2pF in Hz	79577472	7957747	795774	79577	7958	2653	796	79.58
Cutoff Frequency for 20pF in Hz	7957747	795774	79577	7958	795.8	265.3	79.58	7.958
Cutoff Frequency for 50pF in Hz	3183099	318310	31831	3183	318.3	106.1	31.83	3.183
Cutoff Frequency for 100pF in Hz	1591549	159155	15915	1592	159.2	53.05	15.92	1.592
Cutoff Frequency for 200pF in Hz	795775	79577.5	7957.75	795.775	79.5775	26.53	7.95775	0.79575
Cutoff Frequency for 1nF in Hz	159155	15915	1591.5	159.15	15.915	5.305	1.5915	0.15915
Cutoff Frequency for 50nF in Hz	3183	318.3	31.83	3.183	0.3183	0.1061	0.03183	0.003183
Cutoff Frequency for 100nF in Hz	1592	159.2	15.92	1.592	0.1592	0.0531	0.01592	0.001592
Cutoff Frequency for 2pF in s	1.26E-08	1.26E-07	1.26E-06	1.26E-04	1.26E-05	3.80E-06	1.26E-06	1.30E-07
Cutoff Frequency for 20pF in s	1.26E-07	1.26E-06	1.26E-05	1.26E-06	1.26E-06	3.77E-07	1.26E-07	1.30E-08
Cutoff Frequency for 50pF in s	3.14E-07	3.14E-06	3.14E-05	3.14E-06	3.14E-07	1.06E-07	3.14E-08	3.14E-09
Cutoff Frequency for 100pF in s	6.28E-07	6.28E-06	6.28E-05	6.28E-06	6.28E-07	1.89E-07	6.28E-08	6.28E-09

Cutoff Frequency for 200pF in s	1.26E-06	1.26E-05	1.26E-04	1.26E-06	1.26E-06	3.77E-07	1.26E-07	1.30E-08
Cutoff Frequency for 1nF in s	6.28E-06	6.28E-05	6.28E-04	6.28E-06	6.28E-07	1.89E-07	6.28E-08	6.28E-09
Cutoff Frequency for 50nF in s	3.14E-04	3.14E-06	3.14E-05	3.14E-06	3.14E-07	1.06E-07	3.14E-08	3.14E-09
Cutoff Frequency for 100nF in s	6.28E-04	6.28E-06	6.28E-05	6.28E-06	6.28E-07	1.89E-07	6.28E-08	6.28E-09

Appendix D: Example of calibration code

To see the code repository for the CellStat please use the following links.

https://github.com/Dhankism/CellStat.git

Calibration values for each resistance used to modify the code, and update the following parameters in the Python script accordingly:

- QUANT_DAC_TEENSY = 1. /828.33
- OFFSET_DAC_TEENSY = 2069.6
- QUANT_ADC_TEENSY0 = (3.3/4095 * 1.0031=0.00080835897 # Adjust this line for any slope offset for the first resistor
- OFFSET_ADC_TEENSY0 = 2050.3 # Adjust this line for any ADC offset for the first resistor
- QUANT_ADC_TEENSY1 = 3.3/4095 * 1.0169=0.0008195# Adjust this line for any slope offset for the first resistor
- OFFSET_ADC_TEENSY1 = 2044 # Adjust this line for any ADC offset for the first resistor
- QUANT_ADC_TEENSY2 = 3.3/4095 * 1.0160=0.0008188# Adjust this line for any slope offset for the first resistor
- OFFSET_ADC_TEENSY2 = 2045 # Adjust this line for any ADC offset for the first resistor